THE PRC2 MOLECULE EED IS A TARGET OF EPIGENETIC THERAPY FOR NEUROBLASTOMA

(PRC2分子EEDは神経芽腫エピジェネティック 治療の標的である)

By

DILIBAERGULI SHALIMAN

Submitted to Saitama University

Department of Life Science

In partial fulfillment of the requirements for the degree of Doctor of Sciences

Supervisor: Professor Takehiko Kamijo

Saitama, Japan

2022. 9

1.Content

2. Abstract

Epigenetic modifications by polycomb repressive complex (PRC) molecules appear to play a role in the tumorigenesis and aggressiveness of neuroblastoma (NB). Embryonic ectoderm development (EED) is a member of the PRC2 complex that binds to the H3K27me3 mark deposited by EZH2 via propagation on adjacent nucleosomes. We herein investigated the molecular roles of EED in *MYCN*-amplified NB cells using EED-knockdown (KD) shRNAs, EED-knockout sgRNAs, and the EED small molecule inhibitor EED226. The suppression of EED markedly inhibited NB cell proliferation and flat and soft agar colony formation. A transcriptome analysis using microarrays of EED-KD NB cells indicated the de-repression of cell cycle-regulated and differentiation-related genes. The results of a GSEA analysis suggested that inhibitory cell cycle-regulated gene sets were markedly up-regulated. Furthermore, an epigenetic treatment with the EED inhibitor EED226 and the HDAC inhibitors valproic acid/SAHA effectively suppressed NB cell proliferation and colony formation. This combined epigenetic treatment up-regulated cell cycle-regulated and differentiation-related genes. The ChIP sequencing analysis of histone codes and PRC molecules suggested an epigenetic background for the de-repression of down-regulated genes in *MYCN*-amplified/PRC2 up-regulated NB.

3. Introduction

1. Cancer

Cancer is a collection of very complex diseases that share many traits while differing in many ways as well. This makes a universal cure difficult to attain, and it highlights the importance of understanding each type of cancer at a molecular level [1]. The most well-defined epigenetic modification existing in cancer to date is DNA methylation [2]. DNA methylation in humans is carried out by three enzymes: DNA methyltransferase 1 (DNMT1), which maintains parental methylation patterns, and DNMT3A and DNMT3B, which regulate de novo methylation [3, 4, 5, 6]. Another way that cancers are epigenetically regulated is through alterations in histone modification. In each cell, nucleus DNA is wrapped around an octamer of histone proteins. These proteins have flexible N-terminal tails that are extensively modified [1]. Moreover, previous discoveries have highlighted the importance of microRNAs in the regulation of cancer [7, 8, 9, 10]. Interestingly, all three types of epigenetic regulation just mentioned are somewhat intertwined [1].

All cancers are caused by somatic mutations; however, understanding of the biological processes generating these mutations is limited. The catalog of somatic mutations from the cancer genome bears the signatures of the mutational process that has been operative [11]. Somatic mutations found in cancer genomics may be the consequence of the intrinsic slight infidelity of the DNA replication machinery, exogenous or endogenous mutagen exposures, enzymatic modification of DNA, or defective DNA repair. In some cancer types, a substantial proportion of somatic mutations are known to be generated by exposures, for example, tobacco smoking in lung cancers and ultraviolet light in skin cancers, or abnormalities of

DNA maintenance, for example, defective DNA mismatch repair in some colorectal cancers. [12, 13]. In addition, DNA damage responses (DDRs) play critical roles in the maintenance of homeostasis, as exemplified by the findings that diverse human diseases, including cancer, are caused by deficiencies in DDR components [14]. The response to DNA double-strand breaks consists of both positive and negative regulatory pathways, which transmit their signals from sensors to effectors to execute cellular responses. DNA repair scaffolds directly modulate the checkpoint signaling pathway in budding yeast. The functions of scaffold-like proteins in the DDC (DNA damage checkpoint) play essential roles in the coordination of cellular responses to maintain homeostasis [15].

2. Polycomb repressive complex (PRC)

Polycomb group (PcG) proteins have long been linked to the occurrence of different forms of cancer. Some of the PRC complex subunits have been found to be over-expressed in a variety of different tumors. Polycomb proteins were initially identified in Drosophila melanogaster as genes important for developmental defects due to misregulation of specific transcriptional cascades that involved key transcription factors, such as the Homeobox protein, this leads to typical homeotic phenotypes [16].

Polycomb proteins play an important role in maintaining and establishing gene expression patterns during cellular differentiation and development [17, 18]. The two main Polycomb Repressive Complexes in mammals are PRC1 and PRC2. PRC1 contains the products of the PcG genes Polycomb, Posterior sex combs, polyhomeotic, Sex combs on midleg, and several other proteins [19]. A major expansion in the number of PRC1 complexes occurred in the vertebrate lineage. The expansion of the Polycomb Group RING Finger (PCGF) protein

family, an essential step for the establishment of the large diversity of PRC1 complexes found in vertebrates, predates the bilaterian-cnidarian ancestor. This means that the genetic repertoire necessary to form all major vertebrate PRC1 complexes emerged early in animal evolution, over 550 million years ago [20]. Human PRC2 core components include the histone methyltransferase, Enhancer of Zest Homolog (EZH2), its known binding partners, suppressor of Zest12 (SUZ12), and Embryonic Ectoderm Development (EED) [21, 22, 23, 24]. Recent comprehensive proteomic studies established that mammalian PRC2 exists in at least two mutually exclusive subtype assemblies, PRC2.1 and PRC2.2, based on their particular associations with several accessory proteins [25, 26, 27, 28, 29]. PRC2 plays a promising role in tumor suppression, as found in pediatric glioblastoma the oncogenic histone H3K27M missense mutation has an inhibitory activity on PRC2 by binding directly in the EZH2 catalytic active site [30, 31]. EZH2 requires the assembly with EED and SUZ12 to activate the H3K27me3, the blocking of these protein-protein interactions possibly serves as a novel approach for inhibiting PRC2-dependent cancer [32, 33].

3. Neuroblastoma

Neuroblastoma (NB) is the most common solid tumor of early childhood and occupies 8% of pediatric malignancies [34]. NB originates from sympathoadrenal lineage precursor cells and is derived from the neural crest [35]. Almost 50% of all NB cases are at high risk for disease relapse and with intensive multimodal therapy, the servile rates are less than 40% [36].

NB develops mainly in the adrenal medulla but also in the sympathetic ganglia. Some cases of NB show spontaneous regression. Particularly, stage 4S, where S stands for “special”, exhibits

spontaneous regression despite multifocal tumors. Another interesting feature is that, with few exceptions, driver gene mutations are rare in NB, while copy number alterations are common, including *MYCN* amplification, 17q gain, and others, suggesting the involvement of epigenetic regulation [37]. Studies have shown that the common DNA variations facilitate the development of a putative genetic model for this developmental childhood cancer. Amplification of *MYCN*, regional loss or gain of chromosomal material is associated with a poor outcome [38, 39].

During induction of *MYCN* to neuroblastoma tumorigenesis, the PRC2 targets were found to be suppressed by the up-regulation of PRC2 [40]. The CRISPR-Cas9 EZH2 knockout in NB cells resulted in decreased H3K27me3 levels and cell viability [41]. The EZH2-mediated differentiation suppression and epigenetic regulation of *CASZ1* were previously reported [42], and EED binds the H3K27me3 mark deposited by EZH2, via propagation on adjacent nucleosomes [43]. In addition, anti-tumor effects were seen with EZH2 inhibition in NB cells [44]. Moreover, in a previous report mentioned that in preventing the NB cells differentiation, the PRC2 core component EZH2 is one of the important regulator molecules in *MYCN* amplified NB cells [45]. Thus, the PRC2 proteins are precious to studying their functions in NB cells, however, very little is known about the function of EED in NB cells.

4. Embryonic ectoderm development (EED)

Among the most abundant protein interaction domains in the human proteome is the WD40 repeat (WDR) domain, with over 360 domains currently annotated. The WDR domain is a typically seven-bladed beta-propeller domain with an overall donut shape. Significantly, the central pore of the WDR domain frequently mediates interactions with peptide regions of key

interaction partners and often has appropriate size and physicochemical features for high-affinity binding to drug-like small molecules. WDR domains are often essential subunits of multiprotein complexes involved in a wide range of signaling pathways including DNA damage sensing and repair, ubiquitin signaling and protein degradation, cell cycle, epigenetic regulation of gene expression, and chromatin organization, immune-related pathways [46].

In the human proteome, the WD40 repeat domain (WDR) is one of the most abundant domains and has a central binding pocket. Recently, two WDR proteins, WDR5 and EED, have been successfully targeted by specific, cell-active, potent, drug-like chemical probes. Drug-like inhibitors targeting the WDR domain of EED antagonize the binding of an activating peptide that is necessary for the proper propagation of the methyl mark deposited by PRC2 [46].

Importantly, EED binds the H3K27me3 mark deposited by EZH2, via allosteric activation of EZH2 ensuring the H3K27me3 propagation on adjacent nucleosomes [47]. In addition, H3K27me3 modification associated with gene repression, in regulating the expression of genes plays a critical role that determining the balance between cell proliferation and differentiation. As a recurrent in many cancer types, alteration of the histone modification level has emerged. Suggesting that either excess or lack of H3K27 methylation can have an oncogenic effect.

In humans, a de-novo mutation in EED has been reported in an individual displaying symptoms similar to those of weaver syndrome [48]. Previously, two transcript variants encoding distinct isoforms have been identified for the EED gene [49].

5. The effect of drugs on EED

The low number of active clinical trials, despite preclinical evidence of the role of epigenetic regulators in NB, underlines the need for advanced preclinical studies in new therapeutic targets and the development of new compounds. Therefore, the design and development of new small molecules remain a great challenge [50]. GSK126 and EPZ6438, a potent, highly selective, small-molecule inhibitor of EZH2 methyltransferase activity, decrease global H3K27me3 levels and reactivate silenced PRC2 target genes [51, 52]. A large body of evidence has shown that there is an increasing interest in disrupting oncogenic protein complexes and exploring WD40 proteins as potential drug targets. For example, the discovery of potent and selective PRC2 inhibitor EED226 and A395, that directly binds to the EED-H3K27me3 binding pocket and upon binding EED induces a conformational change to loss of PRC2 activity [53, 54]. Meanwhile, the combination strategy for other targeted therapies with EED226 is worth further exploring. Moreover, the interaction of EZH2 with EED is required for EZH2's catalytic activity. Inhibition of the EZH2-EED complex thus represents a novel strategy for interfering with the oncogenic potentials of EZH2 by targeting both its catalytic and non-catalytic functions [55]. Differently from other agents targeting a single gene product, epigenetic drugs have chromatin as their target through inhibition of histone deacetylases (HDACs) and DNA methyltransferases (DNMTs) therefore, yet unspecific, they may act upon most or all tumors types, as deregulation of the methylation and deacetylation machinery are a common hallmark of neoplasia. Valproic acid (VPA) has shown potent anti-tumor effects in a variety of in vitro and in vivo systems, and encouraging results in early clinical trials either alone or in combination with demethylating and/or cytotoxic agents [56]. In this study we have treated the combination of EED inhibitor EED226 and VPA/SAHA in

NB cells, to check the effect of those drugs on the function of PRC2 in NB cells.

6. Aim of present study

In this study, we suppressed the function of EED in NB cells by its knockdown (KD), EED-KO, and using the EED inhibitor EED226. Transcriptome analysis of EED-KD cells identified downstream targets of EED. The EED226 + VPA/SAHA treatment exerted additive inhibitory effects on NB cell proliferation. These results highlight the critical oncogenic role of EED in NB cells. The loss of PRC2 functions by the inhibition of EED has potential as a novel therapeutic option for NB, and the combination of PRC2i and HDACi is a promising candidate in epigenetic therapy for advanced NB.

4. Materials and methods

4.1 Cell culture and reagents

The cells used in experiments (human neuroblastoma cell lines) were obtained from the Tohoku University Cell Resource Center, Miyagi, Japan, and the American Type Culture Collection, Manassas, VA, USA. Experimental cells were cultured in RPMI1640 (Wako, Osaka, Japan) supplemented with 50 μg/ml penicillin and 10% heat-inactivated FBS (Gibco™). Cells were cultured at 37 °C in a humid atmosphere with 5% CO_2. Valproic acid (VPA, Wako, Osaka, Japan), SAHA (Vorinostat, Cayman, Ann Arbor, MI, 9 USA), EED226 (Selleck, Houston, TX, USA), and EPZ-6438 (Med Chem Express, Monmouth Junction, NJ, USA) were used.

4.2 Western blotting analysis

For whole-cell extraction cells were lysed in EBC2 buffer (250 mM NaCl, 50 mM Tris (pH 8.0), 0.5% NP 40, 1 mM EGTA, 50 mM $MgCl_2$) with 1μl Benzonase (25 U Benzonase Nuclease, MilliporeSigma) and put on ice 30 min ~ 1 hr, then centrifuged for 15 min, 4 °C, 13000 rpm, the supernatant was collected for protein assay. For cell fractionation, cells were lysed in EMSA buffer (10 mM Tris (pH 7.5), 1 mM EDTA, 0.5% NP40) and centrifuged then the supernatant was collected (Cytosol sample), the pellet was homogenized (Sonication) with 1% SDS lysis buffer (5 mM EDTA, 2 mM Tris (pH 7.5), 1% SDS), centrifuge 25 °C; 13000 rpm, 5 min; Transfer the supernatant (Nuclear sample) into a new tube for protein assay, after protein assay sample buffer was added to the supernatant solution and boiled at 97 °C, 2 min.

Western blotting (WB) experiments were performed as previously described [57]. The antibodies were used for this study in Table1.

4.3 Knockdown of EED, overexpression of EED by lentiviral gene transduction

The pLKO.1-puro vector (shCont), EZH2 shRNAs (shEZH2-1: TRCN0000018365, sh-EZH2-2: TRCN0000010475), and EED shRNAs (shEED-1: TRCN0000021205, shEED-2: TRCN0000021206) were from MISSON shRNA Library (Sigma-Aldrich). The method used to prepare shRNA lentiviruses was previously described [58]. NGP or IMR32 cells were infected using lentivirus solution with 4 μg/ml polybrene (Sigma- Aldrich). pCDH-FLAG-hEED and pCDH-CMV-MCS-EF1 were used to overexpress EED in IMR32 and SK-N-SH cells. Cells were collected for WB or PCR on Day 10 of virus infection.

4.4 Immunoprecipitation experiment

The nuclear fraction was extracted using nuclear extract buffer (10 mM Tris (pH 7.5), 1 mM EDTA, and 0.5% NP40) with 2 mM PMSF and 1 mM DTT as previously described [57]. A total of 1.5 mg of the nuclear fraction was mixed well in 0.2 ml of lysis buffer (150 mM NaCl, 20 mM HEPES (pH 7.4), 7.5 mM $MgCl_2$, 1 mM EGTA, 2% Tween 20, and 50 mM $MgCl_2$) with 1/100 (v/v) of protease inhibitors (Protease Inhibitor Cocktail for use with mammalian cell and tissue extracts, Nacalai Tesque, Japan), phosphatase inhibitors (2 mM PMSF, 1 mM NaF, 0.1 mM Na_3VO_4, and 1 mM β-glycerophosphate), and 25 U of benzonase (Novagen, Denmark); the above mixture was incubated on ice for 1 hr. The tube was centrifuged at 13,000 rpm at 4 ◦C for 15 min, and the supernatant (sup-B) was collected in a 1.5-ml tube. Protein G (GE Healthcare, Chicago, IL, USA) beads were washed three times in lysis buffer, and a final concentration of 1 μg/ml BSA and 1 μg of the primary antibody were

added to the 1.5-ml tube, which was then incubated at 4 ◦C with shaking on a rotator for 1 hr. Primary antibody-conjugated beads and sup-B were incubated at 4 ◦C overnight and then pelleted by centrifugation at 13,000 rpm at 4 ◦C for 5 min. The precipitates obtained were washed with lysis buffer/1 mM PMSF three times at 4 ◦C, re-suspended in 40 μl of SDS sample buffer, and treated at 100 ◦C for 5 min. Proteins were then resolved by 10% SDS–PAGE and transferred onto Immobilon-P membranes (Millipore, Burlington, MA, USA). The protein complex was detected by WB.

4.5 Semi-quantitative RT-PCR

The method for semi-quantitative RT-PCR was previously described [45, 57]. Primer information is shown in Table 2.

4.6 WST-8 cell proliferation assay

NB cells were seeded on 96-well plates at a density of 10^3 cells/well in a final volume of 100 μl. The culture was maintained under 5% CO2, 10 μl of WST-8 (WST: water-soluble tetrazolium salt) labeling solution (Cell counting Kit-8; DOJINDO, Kumamoto, Japan) was added, and cells were returned to the incubator for 2 hours. The absorbance of the formazan product that formed was detected at 450 nm using a 96-well spectrophotometric plate reader, as per the manufacturer's protocol.

4.7 Flat colony formation assay

Cells were seeded on 6-well in a final volume of 3 ml. The medium was changed every 3

days. EED overexpressed 800 IMR32 cells were seeded in 6 well plates, cultured for 12 days, 1000 cells of EED overexpressed SK-N-SH were seeded in 6 cm dishes, cultured for 14 days, while seeded 300 IMR32 and NGP cells in 6 well plates for checking the effect of EED226 + VPA/SAHA treatment on PRC2 function, cultured 12 days. For colony staining, after removing the cell culture media stained in 1.5 ml/6 cm dish, 800 µl/well of 6 well plates May - Grunwald`s Stain Solution (Room temperature 10 min); remove the May - Grunwald`s Stain Solution and washed with MQ water; stained in 1ml diluted Giemsa`s Azur Eosine Methylene Blue Solution in MQ water (1:20) (Room temperature 30 min). Removed Giemsa`s Azur Eosine Methylene Blue Solution and washed in 1 ml MQ water; in the end, dried up the stained clones in the plate then took the photo by ImageQuent™Las4000, and counted the colony numbers by ImageQuant TL software (Fuji Film, Tokyo, Japan).

4.8 Soft agar colony formation assay

Soft agar colony formation was performed as previously described [59]. 2 × RPMI was prepared (RPMI : NaHCO3 - 13 : 1 in MQ water and added 1/100 volume of Penicillin-Streptomycin Solution) and filtered, then stocked in 4 °C. 1% agar prepared (0.001 g Difco™ agar Noble/ml in MQ water) and Autoclaved. 3 ml bottom agar was prepared in 3.5 ml dish (20% FBS in prepared 2 × RPMI : 1% Agar - 1 : 1, solutions kept in 43.5 °C water bath machine before put into the dishes, for moister used 100 µl Benzalkonium Chloride in 3 ml MQ water), incubated in 37 °C overnight. On the next day IMR32 cell line 2000 cell / 3.5 ml dish, NGP cell line 500 cell/3.5 ml dish, SK-N-SH cell line 20000 cell/3.5 ml dish was seeded in 2 ml (4.5 ml RPMI with cell plus 9 ml 20% FBS in prepared 2 × RPMI : 1% Agar - 1 : 1,

20% FBS in prepared 2 × RPMI : 1% Agar - 1 : 1 was kept in 43 °C before use) solution and cultured in 37 °C for 21 days. The colonies were stained in 0.05 mg/ml MTT in PBS 4 hr ~ overnight, then took the photo and counted colony numbers were in the same way as the flat colony formation assay.

4.9 EED-KO by Edit-R inducible Cas9 system in human neuroblastoma cells NGP and IMR32

The protocol of CRISPR-Cas9 Genome Engineering with Dharmacon™ Edit-R™ inducible Lentiviral Cas9 Nuclease (Horizon™) was used. IMR32 and NGP cell lines were the target cells for lentiviral transduction of Cas9, stable Cas9 cells were selected by blasticidin (NGP - 16 μg/ml, IMR32 - 8 μg/ml) then a single clone was isolated and expanded; the inducible Cas9 clonal cell line was prepared by lentiviral transduction of single clone expended Cas9 stable cells and lentiviral EED-sgRNA (Dharmacon™ Edit-R™, source clone ID - VSGHSM-26692481, DNA target sequence - GGTGCATTTGGCGTGTTTGT) (sgRNA information in Table 2); bulk cells were selected by puromycin (NGP cell 10 μg/ml, IMR32 cell 5 μg/ml); doxycycline (100 ng/ml) was inducted to the bulk cell for EED knockout after all the analyses the EED knockout cells. In this study the -doxy cell means did not occur EED knockout cell, and +doxy means EED knocked out cell.

4.10 Transcriptome analysis

RNA was extracted in Day10 after shEED-expressing lentiviral infection. Using the extracted total RNAs, a microarray analysis was performed using the Agilent platform of 8 x 60 K design ID G4851B (Agilent Single Color. 39494, Agilent Technologies, Santa Clara, CA, USA). Two hundred nanograms of total RNA were labeled with cyanine 3 using a Low

Input Quick-Amp Labeling Kit (One color, Agilent Technologies) according to the manufacturer's instructions.

4.11 Combined treatment of EED226, EPZ6438 and Valproic acid to NB cells

IMR32 and NGP cells were seeded at 5 x 10^5 cells per 10 cm culture plates. On the next day, 10 ml of 10% FBS containing RPMI1640 medium were replaced and 1 mM or 2.5 mM Valproic acid (Wako, Osaka, Japan) and/or, 2 μM EED226 (Selleck, Houston, TX, USA), 2 μM EPZ-6438 (Med Chem Express, Monmouth Junction, NJ, USA) was added. In 3 days after treatment, cells were collected and suspended into ISOGEN II and were extracted total RNAs.

4.12 Statistical analysis

Data are shown as the mean ± standard deviation (SD). Statistical comparisons were performed by the unpaired two-tailed Student's t-test, with $p < 0.05$ indicating significance.

5. Result

5.1 The PRC2 group proteins are the nuclear proteins in NB cells

Polycomb Group (PcG) proteins are transcriptional repressors that play roles in cell differentiation, development, and cell identity maintenance. The role of PcG in NB tumor genesis and aggressiveness has been clarified, EZH2 plays important role in regulating the NB cell differentiation [45]. EZH1, a homolog of EZH2 also catalyzes H3K27 methylation and controls *MYCN* function in NB [60]. EED is shared EZH2 and EZH1 containing PRC2s. These are indicated that EED is an important target of NB therapy. Thus, we detected subcellular localization of PRC2 core components in 5 NB cells by western blotting experiment after cell fractionation. As the result, the PRC2 core components expression levels were high in *MYCN* amplified NGP, IMR32, SK-N-BE cells and *MYCN* not amplified NB-69, SK-N-AS cells compare to 293T cell, and PRC2 proteins were mainly expressed in the nucleus of the NB cells. We detected the 3 isoforms of EED, these are variant 1 (49 KD), variant 2 (46 KD), and variant 3 (52 KD) using the antibody in material and methods (Figure 1A). We then examined the effect of EZH2-KD using lentivirus-mediated shEZH2-1 and shEZH2-2 on EED, SUZ12, and H3K27me. The results of WB revealed that in the whole-cell lysates of IMR32 and NGP cells, reductions were observed in the expression levels of SUZ12, whereas only slight decreases were noted in those of EED. H3K27me1/me2/me3 were decreased after EZH2-KD (Figure 1B). Notably, in the semi-quantitative RT-PCR result, *EED* and *SUZ12* mRNA levels were not decreased by EZH2-KD in IMR32 or NGP cells (Figure 1C). These results indicated that PRC2 proteins worked mainly in the nucleus of NB cells and knockdown of EZH2 reduced H3K27me1/me2/me3. Compare to SUZ12, EED

variants were not reduced clearly by EED knockdown in NB cells.

5.2 EED-KD suppressed NB cell proliferation

We knocked down the EED by lentivirus-mediated shEED-1 and shEED-2 transduction in NGP cells (shEED information in Table 3, Figure 6 for the shRNA recognition sites). With the depletion of EED, The amount of EZH2, SUZ12, H3K27me1, H3K27me2, and H3K27me3 were reduced. H3 amounts were decreased (Figure 2A). When overexpressed EED slightly increased the EZH2 and SUZ12. EZH2, SUZ12 interacted with EED in IMR32 cells, however, not obvious in SK-N-SH cells (Figure 2H, G) (EED variant information in Table 4). Furthermore, in a flat colony formation assay, EED-KD cells formed significantly fewer colony numbers than control (Figure 2B). Moreover, in cell proliferation assay with WST, the proliferation of EED-KD cells was reduced than shCont (Figure 2C). At the mRNA level, *EZH2* and *SUZ12* were not decreased in EED-KD cells (Figure 2D). Target exons of shEED in Figure 6. These results suggested that knockdown of EED suppressed NB cell proliferation and reduced H3K27me1/me2/me3. EED-KD destabilized PRC2 components such as EZH2, SUZ12.

5.3 Transcriptome analysis for EED-depleted cells

In order to elucidate the effect of the suppression of EED on genome-wide gene expression profiles, we performed a transcriptome analysis using microarray. Eighty-four commonly de-repressed genes in EED knockdown using shEED-1 and shEED-2 were selected by the criteria described in the Material and Methods [Moderate t-test $p<0.05$, fold change (FC) >

2.0] (Figure 3A, B). Among them, we found some cell proliferation or apoptosis-related genes such as *BBC3* (*PUMA*), *JUN*, or *TP53INP1*. Consistent with PRC2 molecule EED knockdown, shEED-1 treated cells were significantly enriched to BENPORATH-PRC2-TARGETS containing genes in GSEA analysis (Figure 3C) (Table 5, 6). In the shEED-1 and shEED-2 treated cells, semi-quantitative RT-PCR results suggested that PRC2 target genes were de-repressed, e.g. *CDKN1C* (*p57KIP2*), *RARB,* and *NTRK1* [45, 61], and cell cycle arrest control gene such as *CDKN1A* (*p21WAF1*) (Figure 3D). On the other hand, NB linage-related genes such as *RET*, *DBH*, cell cycle-related kinase *CDK1* and *CDK2* were downregulated. *DBH* was one of the top-ranked genes strongly correlated with 2 years and 5 years of prognosis of neuroblastoma [61]. These results suggested that EED knockdown modified several cell cycle-regulated gene expressions and induced differentiation-related genes in NB cells. In accord with this, GSEA analysis results using both shEED-1 and shEED-2-infected NB cells suggested that cell cycle repressed gene sets (McMURRAY TP53 HRAS COOPERATION RESPONSE DN and WARTERS IR RESPONSE 5GY) were strongly upregulated (Figure 3E) (Table 7).

5.4 EED knockout by CRISPR-Cas9 affected NB cell functions.

To address the EED functions in NB cells, we employed knockout experiments. We knocked out EED from NGP and IMR32 cells by using the doxycycline-inducible CRISPR-Cas9 technique to carry out experiments with good reproducibility as described in Methods. Cas9 expression was induced in the presence of doxycycline as shown in (Figure 4A. a). However, EED depletion was not completely occurred. We picked up more than four clones after sgRNAs infection in both NGP and IMR32 cells and induced Cas9 by doxycycline for

more than 3 weeks (Data not shown). Additionally, the knockout side in the EED sequence was confirmed by the genomic capillary sequencing (Figure 4E). Although EED depletion was not perfect, EZH2, SUZ12, H3K27me1/me2/me3 were clearly decreased in both the EED-KO NGP and IMR32 cells, *EZH2* and *SUZ12* mRNA levels were not changed in the semi-quantitative RT-PCR results (Figure 4A. b). In the flat colony formation assay, the colony-forming efficiency of EED-KO NGP and IMR32 cells was significantly reduced (Figure 4B. a). In the soft agar colony formation experiment, EED-KO cells formed significantly fewer numbers of colonies than control cells (Figure 4B. b), while much more numbers of clones were grown after EED-OE in IMR32 cells than in control cells (Figure 4C). Thus, EED partial depletion by the doxycycline-inducible CRISPR-Cas9 technique resulted in similar results for the EED shRNA-transduced NB cells (Figure 3). Target exons of sgRNA in Figure 6. We used the EED-KO NB cells to study the combined epigenetic therapy development.

5.5 Combination of EED inhibitor EED226 and valproic acid showed synergistic effect on decreasing the NB cell proliferation

We previously found that EZH2 inhibitor and VPA combination suppressed NB cell proliferation [61]. These results prompted us to study the effect of VPA on the PRC2 molecule down-regulated EED-KO cells. Actually, VPA significantly suppressed the cell proliferation of the EED-KO NGP and IMR32 cells (Figure 4D). Next, to develop the epigenetic therapy of NB, we used a small molecule EED inhibitor. EED226 is a potent and selective EED inhibitor that directly binds to the binding pocket of EED and H3K27me3 [63]. According to EED-KO and VPA study, firstly we treated the NGP and IMR32 cells with EED226 after calculating the

IC50 of EED226 for NGP cell 2.64 μM, for IMR32 cell 2.05 μM (Table 8). The result of WST-8 suggested that EED226 or VPA single-treatments suppressed NGP and IMR32 cell proliferation in a dose-dependent manner (Figure 5A). EED226 2μM treatments almost completely diminished the H3K27me3 in NGP and IMR32 cells (Figure 5B). The combination of EED226 and VPA in NGP and IMR32 cells indicated a synergistic effect of these two drugs on the suppression of those cells (Figure 5C). Further, we confirmed this phenomenon by the combination of EED226 and/or SAHA, a potent specific HDAC inhibitor (Figure 5D). These results indicated that suppression of EED activity by a combination of EED226 and VPA could be a new therapy for PRC2-dependent NB. A semi-quantitative RT-PCR experiment (Primer information in Table 2) was performed using RNAs of IMR32 and NGP cells after treatment for 3 days of PRC2is/VPA at the indicated concentration. As the result, growth-associated gene *GAP43*, proapoptotic gene *TP53INP1*, nuclear hormone receptor *RARB*, *NTRK1* (One of the EZH2 mediated epigenetic silencing targets), tumor suppressor gene *CDKN1A* were upregulated by the combination of EED226 and VPA, EPZ6438 and VPA (Figure 5E). While, by VPA or SAHA treatment, H3Ac was increased clearly, however, H3K27me3 levels were not much changed in the NB cell lines (Figure 5F, 5G). We also examined the effects of EEDi and/or HADCi on NB cells in a flat colony formation assay. The results obtained showed that NGP and IMR32 cells treated with the combination of EEDi (EED226) and HADCi (SAHA) formed significantly fewer colonies than those treated with only EEDi (EED226) or HADCi (SAHA) (Figure. 5H). In addition, we investigated the H3K27me3, H3K27ac, H3K4me3, and EZH2 marks using IMR32 parental cell ChIP-sequencing data indicated by Integrative Genomics Viewer software (https://software.broadinstitute.org/software/igv/, Figure 5I). H3K27me3, H3K27ac,

H3K4me3, and EZH2 marks were detected around the promoter regions of *NTRK1* and *c-JUN*, while H3K27me3, H3K4me3, and EZH2 marks were observed at the promoter region of *RARB*, suggesting that the existence of transcription-suppressing H3K27me3/EZH2 marks and loss of transcription-inducing H3K27ac mark may have a role in the de-repression of these genes by the EEDi/HDACi. In contrast, the H3K27ac and H3K4me3 marks were at the *TP53INP1* and *CDKN1C* gene promoter regions, suggesting secondary gene induction by EEDi/HDACi. The *GAPDH* genome view is the control of constitutively expressed genes in *MYCN*-amplified NB because only both H3K4me3 and H3K27ac marks are detected at the promoter region (Figure 5I). These results indicate the potential of the combination of PRC2is and HDACis as a novel therapy for *MYCN*-amplified NB in which PRC2 is up-regulated.

6. Discussion

The Polycomb repressive complexes PRC1 and PRC2 act non-redundantly at target genes to maintain transcriptional programs and ensure cellular identity. PRC2 is a chromatin-associated methyltransferase that catalyzes the mono-, di-, and trimethylation of lysine 27 on histone H3. DNA methylation profiling is commonly used as a diagnostic tool for various cancers. As a key scaffold, EED brings the N-terminal activation loop of EZH2 proximal to the catalytic SET domain to induce basal PRC2 activity [64, 65]. Montgomery et al. previously reported that all four EED variants associated with EZH2 and individual variants of EED were not necessary for H3K27me. EED variants do not control the enzymatic activity of the PRC2 complex. The core WD40 motifs and histone-binding region of EED are sufficient to generate H3K27me1/me2/me3., EED variants 1, 3, and 4 were subsequently detected in a Wap-T121 breast tumor whole-cell extraction sample [66]. A previous study identified EED as a nuclear WD-repeat protein of PcG and a shared component of PRC1 and PRC2 that functions to interchange these epigenetic complexes at sites of histone modifications. In addition, only one band of EED was visible in the prostate cancer cell line DU145 [19]. In the present study, we confirmed that the PRC2 proteins EZH2, SUZ12, and EED variants 1, ×2, and 3 were located in the nuclei of NB cells, and reductions in these variants decreased the levels of the other PRC2 molecules EZH2/SUZ12 and markedly suppressed H3K27me1/me2/me3 (Figure 2A, Figure 4A). EZH2 complexes exhibit differential targeting of specific histones for lysine methylation dependent upon the context of the histone substrates. This differential targeting is a function of the associated EED protein within each complex. EED protein is present in four isoforms, which represent alternate translation start site usage from the same mRNA. These EED isoforms selectively associate

with distinct EZH2-containing complexes with resultant differential targeting of their associated HKMT (Histone lysine methyltransferases) activity toward histone H3-K27 or histone H1-K26 [67]. In mammals, PRC2 acts as a convenience factor to maintain the repressed states of different gene types [68]. Whole-genome studies showed that PRC2 and its mark H3K27me3 captured critical developmental genes in human embryonic stem cells [69]. It has been investigated that, the inhibition of EZH2-induced *NTRK1* expression and EZH2-related *NTRK1* transcriptional regulation is one of the key pathways for suppression of NB differentiation [45]. In the present study, clarified the identity of several downstream targets of EED and showed that reductions in EED up-regulated *NTRK1*, the pro-apoptotic gene *BBC3*, and the tumor suppressor gene *CDKN1A* and down-regulated the proto-oncogene *RET* and the cell proliferation-related genes *DBH*, *CDK1*, and *CDK2* (Figure 3). Additionally, some important cancer related-pathway genes showed significantly different expression profiles. These results suggest that EED is involved in many pathways related to the prevention of NB cell differentiation, and, thus, the inhibition of PRC2 may synergize with drugs that target these pathways. PRC2 plays a promising role in tumor suppression, as demonstrated in pediatric glioblastoma. The oncogenic histone H3K27M missense mutation exhibited inhibitory activity against PRC2 by directly binding to the EZH2 catalytic active site [65, 70]. Loss-of-function studies on individual components of PRC2 have been performed on Drosophila and mice [71, 72, 73]. The deletion of three core PRC2 components, EZH2, SUZ12, and EED, in mice, resulted in severe defects in gastrulation [73], presumably because of reductions in lineage-specific gene expression [74]. While high expression levels of EED correlated with a poor prognosis in NB patients (Figure 7), in the present study, the oncogenic characteristic of EED was confirmed by culture of the EED-KO cells (Figure 4B.

b) and of the EED-overexpressing NB cells (Figure 4C) in a soft agar conditioned environment. Following EED-KO, the EED and H3K27me bands did not completely disappear in WB. A failure to trigger nonsense-mediated mRNA may be one of the causes of ineffective gene inactivation by CRISPR-Cas9 gene editing [75]. Notably, in this study, the sgRNA recognized exon 2 as the target side of EED, and exon 2 is a common exon of all four EED variants (Figure 6).

In a EZH1 and EZH2 knockout form ESC lines by CRISPR-Cas9 system study, loss of EZH1 was fully compensated by EZH2 activity, and EZH2-KO displayed a global loss of both H3K27me2 and H3K27me3 but retained normal H3K27me1 deposition. In addition, all three forms of H3K27 methylation are under EZH1 and EZH2 control in ESCs, H3K27me1 is fully compensated by PRC2-EZH1, and loss of H3K27me2/me3 are always correlated with increased H3K27ac levels [76]. Conditional knockout of EED gene impairs fetal hematopoiesis including erythropoiesis and formation of hematopoietic progenitor and stem cells [77]. Accumulating evidence in the mice model demonstrated that loss-of-function mutations of EED gene might be a potential etiology of leukemia. Ikeda et al., report that EED haploinsufficiency induces hematopoietic dysplasia, and EED heterozygous mice are susceptible to malignant transformation and developed leukemia in cooperation with Evil over-expression [78].

Detailed examinations of the protein families that modify the acetylation and methylation of histones and the proteins that bind to modified histones recently revealed that these targets are druggable. The allosteric inhibition of PRC2 by targeting EED is a promising approach for the development of effective cancer therapy [63], and it has already been established that the H3K27me3 peptide stimulates PRC2 activity by binding to the EED subunit [79]. VPA and

SAHA have emerged as promising drugs for cancer treatments. A combination of quinacrine and SAHA significantly decreased colony formation and increased cancer cell death and the combination was more effective than a single-agent treatment in abrogating tumor growth in vivo [80]. VPA has emerged as a promising drug for cancer treatments. Whole genome expression by microarray analysis of the primary tumors of patients treated with VPA revealed the significantly up-regulated expression of hundreds of genes belonging to multiple pathways, including ribosomal proteins, oxidative phosphorylation, and MAPK signaling. VPA is a potential candidate in combination therapy for malignancies, with classical cytotoxic drugs, other molecular-targeted drugs, or radiation in a number of solid tumor therapies [81]. VPA plus IFN-alpha synergistically inhibited the growth of UKF-NB-3 xenograft tumors in nude mice [82]. Furthermore, in a model of chemotherapy resistance in NB cells, VPA reverted the enhanced adhesion properties of drug-resistant UKF-NB-2, UKF-NB-6, and SK-N-SH cells accompanied by decreased N-myc and increased p73 protein levels [83]. Moreover, a recent study reported that EED226 and EZH2 inhibitors similarly altered the transcriptome, and EED226 inhibited EZH2-resistant PRC2 [62]. The pharmacological inhibition of PRC2 combined with other treatments may lead to the development of novel anticancer therapies [84]. We found that the combination of the EED inhibitor EED226 and VPA additively inhibited the proliferation of NGP and IMR32 cells as well as the synergistic effects of EEDi/HDACi on the de-repression of cell cycle-regulated genes and differentiation-related genes in NB cells (Figure 5D). There is a significant body of prior work demonstrating a role for PRC2 in the maintenance of HIV latency and the potential for EZH2 inhibitors in latency reversal for cure strategy [85]. EED inhibitors are a growing list of agents to be considered for latency reversal studies. While EED inhibitors A-395 and EED226 phenocopy

EZH2 inhibitors with regards to HIV latency reversal, however, EED inhibitors have the potential to be used without blocking PRC2-independent EZH2 activity. The evaluation of EEDi as Latency reversal agentsin (LRAs) resting and total CD4+ T-cells isolated from antiretroviral therapy (ART) suppressed, viremic individuals, is the subject of ongoing work [86].

ChIP sequence data on PRC2- and HDAC-related histone codes suggested an epigenetic mechanism of de-repression (Figure 5E). Epigenetic regulation of gene expression is essential for development and cellular differentiation [87, 88]. PRC2 is recruited to target sites independently of H3K27me3 and H2Aub1 deposition. The activity of EZH1 is sufficient to deposit H3K27me3 at all PRC2 target sites but is unable to spread this modification to neighboring chromatin. Although this is sufficient to fully recruit PRC1 activity at these sites and to prevent hyperacetylation of PcG target promoters, EZH1 activity is unable to counteract diffused chromatin H3K27ac hyperacetylation caused by H3K27me2 loss or to support proper ESC differentiation. Taken together, early developmental failure induced by loss of PRC2 activity is a consequence of chromatin H3K27 hyperacetylation rather than specific loss of repressive control at target genes [76]. As an example of PRC2 function in cancer, several studies about acute myeloid leukemia (LAML) have been reported, since abnormal expression and inactivation of PcG genes have been considered important causes of hematological malignancies including LAML and diffuse large B-cell lymphoma (DLBC) due to the depression of pro-oncogenes [89]. Importantly, high EED mRNA level was associated with poor prognosis and high CALGB cytogenetic risk of LAML patients, EED mRNA level in DLBC cells was higher than control cells, and EED gene expression could be regulated by both copy number alterations and DNA methylation, additionally, there were different EED

co-expression genes nets in the two kinds of hematologic malignancies [89]. In DLBC cells, the high H3K27me3 level is significantly correlated with EZH2 protein level and predicts inferior overall survival [90]. Moreover, Shi et al., report that suppression of PRC2 core genes EED, SUZ12 or EZH1/EZH2 results in proliferation arrest and differentiation of leukemia cells [91].

To the best of our knowledge, this is the first EED functional study of NB. We identified some important downstream target genes of EED, which are responsible for cell proliferation, tumor suppression, apoptosis, and differentiation. The depletion of EED decreased the proliferation of NB cells, which confirmed the oncogenic role of EED in NB. The present results demonstrated the potential of EED as a novel therapeutic target, and the combination of EEDi/HDACi epigenomic therapy may be useful for the treatment of MYCN-amplified NB.

7. Summary

The survival rate of high-risk NB is less than 40% and further studies are needed to develop novel treatments for these patients. In *MYCN*- amplified aggressive NB, the role of PcG molecules has been highlighted by findings showing the *MYCN*-related induction of PcG in NB. In the present study, we examined the molecular roles of EED in *MYCN*- amplified NB cells and found that its suppression by EED-KD, EED-KO, and EEDi markedly inhibited NB cell proliferation/colony formation. The results of the transcriptome analysis indicated the de-repression of NB differentiation-related genes (*RARB*, *NTRK1*, and *GAP43*) and cell cycle arrest/cell death control genes (*CDKN1A* and *TP53INP1*). Furthermore, an epigenetic treatment involving the combination of the EED inhibitor EED226 and HDAC inhibitors VPA/SAHA effectively suppressed NB cell proliferation and colony formation and de-repressed cell cycle arrest/cell death control- and differentiation-related genes. These results will be an important platform for developing epigenetic therapy strategies for *MYCN*-amplified/PcG up-regulated NB tumors.

8. Acknowledgements

I would like to express my deepest appreciation to all those who provided me with the possibility to complete this thesis. A special gratitude I give to my supervisor Professor Takehiko Kamijo, I would like to thank him for allowing me to study independently and grow as a research scientist. His patience, contribution in stimulating suggestions, encouragement, and advice were given to me help not only in my study but also in my daily life. I am also grateful to Dr. Hisanori Takenobu. Furthermore, I would also like to acknowledge with much appreciation the crucial role of the members of the Saitama Cancer Research center. I have to appreciate the suggestions given by all of the teachers as well as all of my labmates in our presentation, which has improved my presentation skills thanks to their comments and advice.

We thank Ms. Kumiko Tachikawa for her technical assistance and Mr. Daniel Mrozek (Medical English Service, Kyoto) for his English editorial assistance.

Data Availability:

Microarray data accession number: GSE183369.

ChIP sequencing data accession number: GSE162059.

Conflicts of interest:

The authors declare that there is no conflict of interest.

9. Reference

1. Blair L. P.; Yan Q. Epigenetic Mechanisms in Commonly Occurring Cancers. *DNA Cell Biol*. **2012**, *31*, 49-61.
2. Paredes M. R; Esteller M. Cancer epigenetics reaches mainstream oncology. *Nat Med.* **2011***, 17,* 330–339.
3. Bestor T. H; Ingram V. M. Two DNA methyltransferases from murine erythroleukemia cells: purification, sequence specificity, and mode of interaction with DNA. *PNAS.* **1983**, *80* 5559-5563.
4. Okano M; Daphne W. B; Daniel A. H; En L. DNA Methyltransferases Dnmt3a and Dnmt3b Are Essential for De Novo Methylation and Mammalian Development. *Cell.* **1999**, *99*, 247-257.
5. Moore L. D.; Le T.; Fan G. DNA Methylation and Its Basic Function. *Neuropsychopharmacology.* **2013**, *38*, 23-38.
6. Moarefi A. H.; Chédin F. ICF syndrome mutations cause a broad spectrum of biochemical defects in DNMT3B-mediated de novo DNA methylation. *J Mol Biol.* **2011**, *409*, 758-72.
7. Braconi C.; Valeri N.; Kogure T.; Gasparini P.; Huang N.; Nuovo G. J.; Terracciano L.; Croce C. M.; Patel T. Expression and functional role of a transcribed noncoding RNA with an ultraconserved element in hepatocellular carcinoma. *Proc Natl Acad Sci U S A.* **2011**, *108*, 786-91.
8. Fabbri M.; Bottoni A.; Shimizu M.; Spizzo R.; Nicoloso M. S.; Rossi S.; Barbarotto E.; Cimmino A.; Adair B.; Wojcik S. E. Association of a MicroRNA/TP53 Feedback Circuitry With Pathogenesis and Outcome of B-Cell Chronic Lymphocytic Leukemia. *JAMA.* **2011***, 305*, 59-67.

9. Ferracin M.; Pedriali M.; Veronese A.; Zagatti B.; Gafà R.; Magri E.; Lunardi M.; Munerato G.; Querzoli G.; Maestri I, Ulazzi L. MicroRNA profiling for the identification of cancers with unknown primary tissue-of-origin. *J Pathol.* **2011**, *255*, 43-53.
10. Landau D. A.; Slack F. J. MicroRNAs in mutagenesis, genomic instability, and DNA repair. *Semin Oncol.* **2011**, *38*, 743-51.
11. Alexandrov L. B.; Serena N. Z.; Michael R. S. Signatures of mutational processes in human cancer. *Nature.* **2013**, *500*, 415-421.
12. Stratton M. R.; , Campbell P. J.; Futreal P. A. The cancer genome. *Nature.* **2009**, *458*, 719-24.
13. Pfeifer G. P. Environmental exposures and mutational patterns of cancer genomes. *Genome Med.* **2010**, *2*, 54.
14. Jackson S. P.; Bartek J. The DNA-damage response in human biology and disease. *Nature.* **2009**, *461*, 1071-8.
15. Ohouo P. Y.; Oliveira F. M. B.; Liu Y.; Ma C. J.; Smolka M. B. DNA-repair scaffolds dampen checkpoint signalling by counteracting the adaptor Rad9. *Nature.* **2013**, *493*, 120-4.
16. Déjardin J.; Rappailles A.; Cuvier O.; Grimaud C.; Decoville M.; Locker D.; Cavalli G. Recruitment of *Drosophila* Polycomb group proteins to chromatin by DSP1. *Nature.* **2005**, *434*, 533-538.
17. Kamijo T. Role of stemness-related molecules in neuroblastoma. *Pediatr. Res*. **2012**, *71*, 511–515.
18. Pinto N. R.; Applebaum M. A.; Volchenboum S. L.; Matthay K. K.; London W. B.; Ambros P F.; Nakagawara A.; Berthold F.; Schleiermacher G.; Park J. R.; et al. Advances

in Risk Classification and Treatment Strategies for Neuroblastoma. *J. Clin. Oncol*. **2015**, *33*, 3008–3017.

19. Shao Z.; Raible F.; Mollaaghababa R.; Guyon J. R.; Wu C.; Bender W.; Kingston R. E. Stabilization of chromatin structure by PRC1, a Polycomb complex. *Cell.* **1999**, *98*, 37-46.
20. Gahana J. M.; Rentzsch F; Schnitzler C. E. The genetic basis for PRC1 complex diversity emerged early in animal evolution. *PNAS.* **2020**, *117*, 22880-22889.
21. Yoo K. H.; Hennighausen L. EZH2 Methyltransferase and H3K27 Methylation in Breast Cancer. *Int J Biol Sci.* **2012**, *8*, 59-65.
22. Chase A.; Cross N. C. P. Aberrations of *EZH2* in Cancer. *Clin Cancer Res*. **2011**, *17*, 2613-2618.
23. Herz H. M.; Garruss A.; Shilatifar A. SET for life: biochemical activities and biological functions of SET domain-containing proteins. *Trends Biochem. Sci.* **2013**, *38*, 621-639.
24. Can r.; Zhang Y. SUZ12 is required for both the histone methyltransferase activity and the silencing function of the EED-EZH2 complex. *Mol. Cell*. **2004**, *15*, 57-67.
25. Healy E.; Mucha M; Glancy E.; Fitzpatrick D. J.; Conway E.; Neikes H. K.; Monger C.; Mierlo G. V.; Baltissen M. P.; Koseki Y.; et al. PRC2.1 and PRC2.2 Synergize to Coordinate H3K27 Trimethylation. *Mol. cell.* **2019**, *76*, 437-452.
26. Grijzenhout A.; Godwin J.; Koseki H.; Gdula M. R.; Szumska D.; McGouran J. F.; Bhattacharya S.; Kessler B. M.; Brockdorff N.; Cooper S. Functional analysis of AEBP2, a PRC2 Polycomb protein, reveals a Trithorax phenotype in embryonic development and in ESCs. *Development.* **2016**, *143*, 2716-23.
27. Hauri S.; Comoglio F.; Seimiya M.; Gerstung M.; Glatter T.; Hansen K.; Aebersold

R.; Paro R.; Gstaiger M.; Beisel C. A High-Density Map for Navigating the Human Polycomb Complexome. *Cell Rep.* **2016**, *17*, 583-595.

28. Laugesen A.; Højfeldt J. W.; Helin K. Molecular Mechanisms Directing PRC2 Recruitment and H3K27 Methylation. *ScienceDirect.* **2019**, *74*, 8-18.
29. Streubel G.; Watson A.; Jammula S. G.; Scelfo A.; Fitzpatrick D. J.; Oliviero G.; McCole R.; Conway E.; Glancy E.; Negri G. L. The H3K36me2 Methyltransferase Nsd1 Demarcates PRC2-Mediated H3K27me2 and H3K27me3 Domains in Embryonic Stem Cells. *Mol Cell.* **2018**, *70*, 371-379.
30. Peifer M.; Hertwig F.; Roels F.; Dreidax D.; Gartlgruber M.; Menon R.; Krämer A.; Roncaioli J. L.; Sand F.; Heuckmann J. M.; et al. Telomerase activation by genomic rearrangements in high-risk neuroblastoma. *Nature*. **2015**, *526*, 700–704.
31. Pugh T. J.; Morozova O.; Attiyeh E. F.; Asgharzadeh S.; Wei J. S.; Auclair D.; Carter S. L.; Cibulskis K.; Hanna M.; Kiezun A.; et al. The genetic landscape of high-risk neuroblastoma. *Nat. Genet.* **2013**, *45*, 279–284.
32. Kamijo T.; Koike K.; Nakazawa Y.; Takeuchi K.; Ishii E.; Komiyama A. Synergism between stem cell factor and granulocyte-macrophage colony-stimulating factor on cell proliferation by induction of cyclins. *Cytokine*. **2002**, *19*, 267-275.
33. Teitz T.; Wei T.; Valentine M. B.; Vanin E. F.; Grenet J.; Valentine V. A.; Behm F. G.; Look A. T.; Lahti J. M.; Kidd V. J. Caspase 8 is deleted or silenced preferentially in childhood neuroblastomas with amplification of *MYCN*. *Nat. Med.* **2000***, 6,* 529–535.
34. Haruta M.; Kamijo T.; Nakagawara A.; Kaneko Y. *RASSF1A* methylation may have two biological roles in neuroblastoma tumorigenesis depending on the ploidy status and age of patients. *Cancer Let.* **2014**, *348*, 167-176.

35. Margueron R.; Reinberg D. The Polycomb complex PRC2 and its mark in life. *Nature.* **2011**, *469*, 343–349.

36. Simon J. A.; Kingston R. E. Mechanisms of polycomb gene silencing: knowns and unknowns. *Nat. Rev. Mol. Cell Biol.* **2009**, *10*, 697–708.

37. Pugh T. J.; et al. The genetic landscape of high-risk neuroblastoma. *Nat Genet.* **2013**, *45*, 279-84.

38. Cao R.; Wang L.; Wang H.; Xia L.; Erdjument-Bromage H.; Tempst P.; Jones R. S.; Zhang Y. Role of histone H3 lysine 27 methylation in Polycomb-group silencing. *Science*. **2002**, *298*, 1039–1043.

39. Kuzmichev A.; Jenuwein T.; Tempst P.; Reinberg D. R. Different EZH2-containing complexes target methylation of histone H1 or nucleosomal histone H3. *Mol. Cell.* **2004**, *14*, 183–193.

40. Chen H.; Gao S.; Li J.; Liu D.; Sheng C.; Yao C.; Jiang W.; Wu J.; Chen S.; Huang W. Wedelolactone disrupts the interaction of EZH2-EED complex and inhibits PRC2-dependent cancer. *Oncotarget.* **2015**, *6*, 13049–13059.

41. Tsubota S.; Kishida S.; Shimamura T.; Ohira M.; Yamashita S.; Cao D.; Kiyonari S.; Ushijima T.; Kadomatsu K. PRC2-Mediated Transcriptomic Alterations at the Embryonic Stage Govern Tumorigenesis and Clinical Outcome in MYCN-Driven Neuroblastoma. *Cancer Res*. **2017**, *77*, 5259-5271.

42. Huang F.; Pan B.; Wu J.; Chen E.; Chen L. Relationship between exposure to PM2.5 and lung cancer incidence and mortality: A meta-analysis. *Oncotarget*. **2017**, *8*, 43322–43331.

43. Margueron R.; Justin N.; Ohno K.; Sharpe M. L.; Son J.; Drury W. J. 3rd; Voigt P.; Martin S. R.; Taylor W. R.; De Marco V.; Pirrotta V.; Reinberg D.; Gamblin S. J. Role of the

polycomb protein EED in the propagation of repressive histone marks. *Nature.* **2009**, 461, 762–767.

44. Wang C.; Liu Z.; Chan-Wook W, Li Z.; Wang L.; Wei J. S.; Marquez V. E.; Bates S. E.; Jin Q.; Khan J.; et al. EZH2 Mediates epigenetic silencing of neuroblastoma suppressor genes CASZ1, CLU, RUNX3, and NGFR. *Cancer Res*. **2012**, *72*, 315-324.
45. Li Z.; Takenobu H.; Setyawati A. N.; Akita N.; Haruta M.; Sato S.; Shinno Y.; Chikaraishi K.; Ohira M.; Akter J.; et al. EZH2 regulates neuroblastoma cell differentiation via NTRK1 promoter epigenetic modifications. *Oncogene*. **2018**, *37*, 2714–2727.
46. Cao R.; Zhang Y. SUZ12 is required for both the histone methyltransferase activity and the silencing function of the EED-EZH2 complex. *Mol. Cell.* **2004**, *15*, 57–67.
47. Kim W.; Bird G. H.; Neff T.; Guo G.; Kerenyi M. A.; Walensky L. D.; Orkin S. H. Targeted disruption of the EZH2-EED complex inhibits EZH2-dependent cancer. *Nat. Chem. Biol.* **2013**, *9*, 643–650.
48. Cohen A. S. A.; Tuysuz B.; Shen Y.; Bhalla S. K.; Jones S J. M.; Gibson W. T. A novel mutation in *EED* associated with overgrowth. *Journal of Human Genetics.* **2015**, *60*, 339–342.
49. Pruitt K. D.; Tatusova T.; Klimke W.; Maglott D. R. NCBI Reference Sequences: current status, policy and new initiatives. *Nucleic Acids Res.* **2009**, 37.
50. Bownes L. V.; Williams A. P.; Marayati R.; Stafman L. L.; Markert H.; Quinn C. H.; Wadhwani N.; Aye J. M.; Stewart J. E.; Yoon K. J.; et al. EZH2 inhibition decreases neuroblastoma proliferation and *in vivo* tumor growth. *PLoS ONE*. **2021**, *16*, e0246244.
51. Margueron R.; Justin N.; Ohno K.; Sharpe M. L.; Son J.; Drury W. J.; Voigt P.; Martin S. R.; Taylor W. R.; De Marco V.; et al. Role of the polycomb protein EED in the

propagation of repressive histone marks. *Nature.* **2009***, 461*, 762-767.

52. Jubierre L.; Jiménez C.; Rovira E.; Soriano A.; Sábado C.; Gros L.; Llort A.; Hladun R.; Roma J.; Toledo J. S.; et al. Targeting of epigenetic regulators in neuroblastoma. *Exp. Mol. Med.* **2018**, *50*, 1-12.
53. McCabe M. T.; Ott H. M.; Ganji G.; Korenchuk S.; Thompson C.; Van Aller G. S.; Liu Y.; Graves A. P.; Della Pietra A.; Diaz E.; et al. EZH2 inhibition as a therapeutic strategy for lymphoma with EZH2-activating mutations. *Nature*. **2012,** *492*, 108–112.
54. Knutson S. K.; Kawano S.; Minoshima Y.; Warholic N. M.; Huang K. C.; Xiao Y.; Kadowaki T.; Uesugi M.; Kuznetsov G.; Kumar N.; et al. Selective Inhibition of EZH2 by EPZ-6438 Leads to Potent Antitumor Activity in *EZH2*-Mutant Non-Hodgkin Lymphoma. *Small Mol. Ther*. **2014**, *13*, 842-854.
55. Zhu M. R.; Du D.; Hu J.; Li L.; Liu J.; Ding H.; Kong X.; Jiang H.; Chen K.; Luo C. Development of a high-throughput fluorescence polarization assay for the discovery of EZH2-EED interaction inhibitors. *Acta Pharmacologica Sinica.* **2018**, *39*, 302–310.
56. Candelaria M.; Gallardo-Rincón D.; Arce C.; Cetina L.; Aguilar-Ponce J. L.; Arrieta O.; González-Fierro A.; Chávez-Blanco A.; Cruz-Hernández E.; Camargo M. F.; et al. A phase II study of epigenetic therapy with hydralazine and magnesium valproate to overcome chemotherapy resistance in refractory solid tumors. *Ann. Oncol.* **2007**, *18*, 1529-1538.
57. Kurata K.; Yanagisawa R.; Ohira M.; Kitagawa M.; Nakagawara A.; Kamijo T. Stress via p53 pathway causes apoptosis by mitochondrial Noxa upregulation in doxorubicin-treated neuroblastoma cells. *Oncogene*. **2008**, *27*, 741–754.
58. Ochiai H.; Takenobu H.; Nakagawa A.; Yamaguchi Y.; Kimura M.; Ohira M.; Okimoto Y.;

Fujimura Y.; Koseki H.; Kohno Y.; et al. Bmi1 is a MYCN target gene that regulates tumorigenesis through repression of KIF1B β and TSLC1 in neuroblastoma. *Oncogene*. **2010**, *29*, 2681–2690.

59. Takenobu H.; Shimozato O.; Nakamura T.; Ochiai H.; Yamaguchi Y.; Ohira M.; Nakagawara A.; Kamijo T. CD133 suppresses neuroblastoma cell differentiation via signal pathway modification. *Oncogene*. **2011**, *30*, 97–105.
60. Shinno Y.; Takenobu H.; Sugino R.; Endo Y.; Okada R.; Haruta M.; Satoh S.; Mukae K.; Shaliman D.; Wada T.; et al. Polycomb EZH1 regulates cell cycle/5-FU sensitivity of neuroblastoma cells in concert with MYCN. In preparation.
61. Endo Y.; Takenobu H.; Kamijo T.; et al. In preparation.
62. Ohira M.; Oba S.; Nakamura Y.; Isogai E.; Kaneko S.; Nakagawa A.; Hirata T.; Kubo H.; Goto T.; Yamada S.; et al. Expression profiling using a tumor-specific cDNA microarray predicts the prognosis of intermediate risk neuroblastomas. *Cancer Cell*. **2005**, *7*, 337-350.
63. Qi W.; Zhao K.; Gu J.; Huang Y.; Wang Y.; Zhang H.; Zhang M.; Zhang J.; Yu Z.; Li L.; et al. An allosteric PRC2 inhibitor targeting the H3K27me3 binding pocket of EED. *Nat. Chem. Biol.* **2017**, *13*, 381–388.
64. Justin N.; Zhang Y.; Tarricone C.; Martin S. R.; Chen S.; Underwood E.; De Marco V.; Haire L F.; Walker P A.; Reinberg D.; et al. Structural basis of oncogenic histone H3K27M inhibition of human polycomb repressive complex 2. Gamblin. *Nat. Commun.* **2016,** *7*, 11316.
65. Jiao L.; Liu X. Structural basis of histone H3K27 trimethylation by an active polycomb repressive complex2. *Science*. **2015**, *350*, 4383.

66. Montgomery N. D.; Yee D.; Montgomery S. A.; Magnuson T. Molecular and functional mapping of EED motifs required for PRC2-dependent histone methylation. *J. Mol. Biol*. **2007**, *374*, 1145-1157.

67. Kirmizis A.; Bartley S M.; Kuzmichev A.; Margueron A.; Reinberg D.; Green R.; Farnham P J. Silencing of human polycomb target genes is associated with methylation of histone H3 Lys . *Genes Dev.* **2004**, *18*, 1592-605.

68. Cao Q.; Wang X.; Zhao M.; Yang R.; Malik R.; Qiao Y.; Poliakov A.; Yocum AK.; Li Y.; Chen W.; et al. The Central Role of EED in the Orchestration of Polycomb Group Complexes. *Nat. Commun*. **2014**, *5*, 3127.

69. Lee T. I.; Jenner R. G.; Boyer L. A.; Guenther M. G.; Levine S. S.; Kumar R. M.; Chevalier B.; Johnstone S. E.; Cole M. F.; Isono K.; et al. Control of developmental regulators by Polycomb in human embryonic stem cells. *Cell.* **2006***, 125*, 301–313.

70. Kui-Ming C.; Fang D.; Gan H.; Hashizume R.; Yu C.; Schroeder M.; Gupta N.; Mueller S.; James C D.; Jenkins R.; et al. The histone H3.3K27M mutation in pediatric glioma reprograms H3K27 methylation and gene expression. *Genes Dev.* **2013***, 27*, 985-990.

71. Müller J.; Hart C. M.; Francis N. J.; Vargas M. L.; Sengupta A.; Wild B.; Miller E. L.; O'Connor M. B.; Kingston R. E.; Simon J. A. Histone methyltransferase activity of a *Drosophila* Polycomb group repressor complex. *Cell*. **2002**, *111*, 197–208.

72. Czermin B.; Melfi R.; McCabe D.; Seitz V.; Imhof A.; Pirrotta V. Drosophila enhancer of Zeste/ESC complexes have a histone H3 methyltransferase activity that marks chromosomal polycomb sites. *Cell.* **2002**, *111*, 185–196.

73. Carroll O.; Erhardt S.; Pagani M.; Barton S. C.; Surani M. A.; Jenuwein T. The polycomb-group gene Ezh2 is required for early mouse development. *Mol. Cell. Biol.* **2001**, *21*,

4330–4336.

74. Faust C.; Schumacher A.; Holdener B.; Magnuson T. The eed mutation disrupts anterior mesoderm production in mice. *Development*. **1995,** *121*, 273-285.
75. Lindeboom R. G. H.; Vermeulen M.; Lehner B.; Supek F. The impact of nonsense-mediated mRNA decay on genetic disease, gene editing and cancer immunotherapy. *Nat. Genet*. **2019,** *51*, 1645–1651.
76. Lavarone E.; Barbieri C M.; Pasini D. Dissecting the role of H3K27 acetylation and methylation in PRC2 mediated control of cellular identity. *Nature Communications*. **2019**, *10*, 1679.
77. Yu W.; Zhang F.; Wang S.; Fu Y.; Chen J.; Liang X.; Le H.; Pu W T.; Zhang B. Depletion of polycomb repressive complex 2 core component EED impairs fetal hematopoiesis. *Cell Death Dis*. **2017**, *8*, e2744.
78. Ikeda A, Kajiwara K, Iwamoto K, Makino A, Kobayashi T, Mizuta K, Funato K. Complementation analysis reveals a potential role of human ARV1 in GPI anchor biosynthesis. *Yeast*. **2016**, *33*, 37-42.
79. Xu C.; Bian C.; Yang W.; Galka M.; Ouyang H.; Chen C.; Qiu W.; Liu H.; Jones A. E.; MacKenzie F.; et al. Binding of different histone marks differentially regulates the activity and specificity of polycomb repressive complex 2 (PRC2). *Proc. Natl. Acad. Sci. U.S.A*. **2010***, 107*, 19266-19271.
80. Zhu, S.; Chen, Z.; Wang, L.; Peng, D.; Belkhiri, A.; Lockhart, C.; EI-Rifai, W. A Combination of SAHA and Quinacrine Is Effective in Inducing Cancer Cell Death in Upper Gastrointestinal Cancers. *Clin. Cancer Res*. **2018**, *24*, 1905-1916.
81. Duenas-Gonzalez A.; Candelaria M.; Perez-Plascencia C.; Perez-Cardenas E.; de la Cruz-

Hernandez E.; Herrera L. A. Valproic acid as epigenetic cancer drug: Preclinical, clinical and transcriptional effects on solid tumors. *Cancer Treat. Rev.* **2008**, *34*, 206– 222.

82. Michaelis M.; Michaelis U. R.; Fleming I.; Suhan T.; Cinatl J.; Blaheta R. A.; Hoffmann K.; Kotchetkov R.; Busse R.; Nau H.; et al. Valproic acid inhibits angiogenesis in vitro and in vivo. *Mol. Pharmacol.* **2004**, *65*, 520-527.
83. Blaheta R. A.; Michaelis M.; Natsheh I.; Hasenberg C.; Weich E.; Relja B.; Jonas D.; Doerr H. W.; Cinatl Jr J. Valproic acid inhibits adhesion of vincristine- and cisplatin-resistant neuroblastoma tumour cells to endothelium. Br. J. Cancer. **2007**, *96*, 1699–1706.
84. Shi Y.; Xiao-xi W.; You-wen Z.; Yi J.; Melcher K.; Xu E. H. Structure of the PRC2 complex and application to drug discovery. *Acta Pharmacol. Sin.* **2017**, *38*, 963–976.
85. Turner Anne-Marie W.; Margolis D M. Chromatin Regulation and the Histone Code in HIV Latency. *Yale J Biol Med.* **2017**, *90*, 229-243.
86. Margolis D. M.; Archin N. M.; Cohen M. S.; Eron J. J.; Ferrari G.; Garcia J. V.; Gay C. L.; Goonetilleke N.; Joseph S. B.; Swanstrom R.; et al. Curing HIV: Seeking to Target and Clear Persistent Infection. *Cell.* **2020**, *181*, 189-206.
87. Zhou V. W.; Goren A, Bernstein B. E. Charting histone modifications and the functional organization of mammalian genomes. *Nat Rev Genet.* **2011**, *12*, 7-18.
88. Creyghton M. P.; Cheng A. W.; Welstead G. G.; Kooistra T, Carey B. W, Steine E. J.; Hanna J.; Lodato M. A.; Frampton G. M.; Sharp P. A.; et al. Histone H3K27ac separates active from poised enhancers and predicts developmental state. *Proc Natl Acad Sci U S A.* **2010**, *107*, 21931-6.
89. Yu W.; Du H. Roles of Polycomb gene EED in pathogenesis and prognosis of acute

myeloid leukemia and diffuse large B cell lymphoma. *bioRxiv.* **2018**, DOI:10.1101/444745.

90. Oh E. J.; Yang W. I.; Cheong J. W.; Choi S. E.; Yoon S. O. Diffuse large B-cell lymphoma with histone H3 trimethylation at lysine 27: another poor prognostic phenotype independent of c-Myc/Bcl2 coexpression. *Hum Pathol.* **2014**, *45*, 2043-50.
91. Junwei Shi J.; Eric Wang E.; Zuber J.; Rappaport A.; Taylor M.; Johns C.; Lowe, S. W.; Vakoc C. R. The Polycomb complex PRC2 supports aberrant self-renewal in a mouse model of MLL-AF9;NrasG12D acute myeloid leukemia. *Oncogene.* **2013**, *32*, 930-938.

10. Figures and Tables

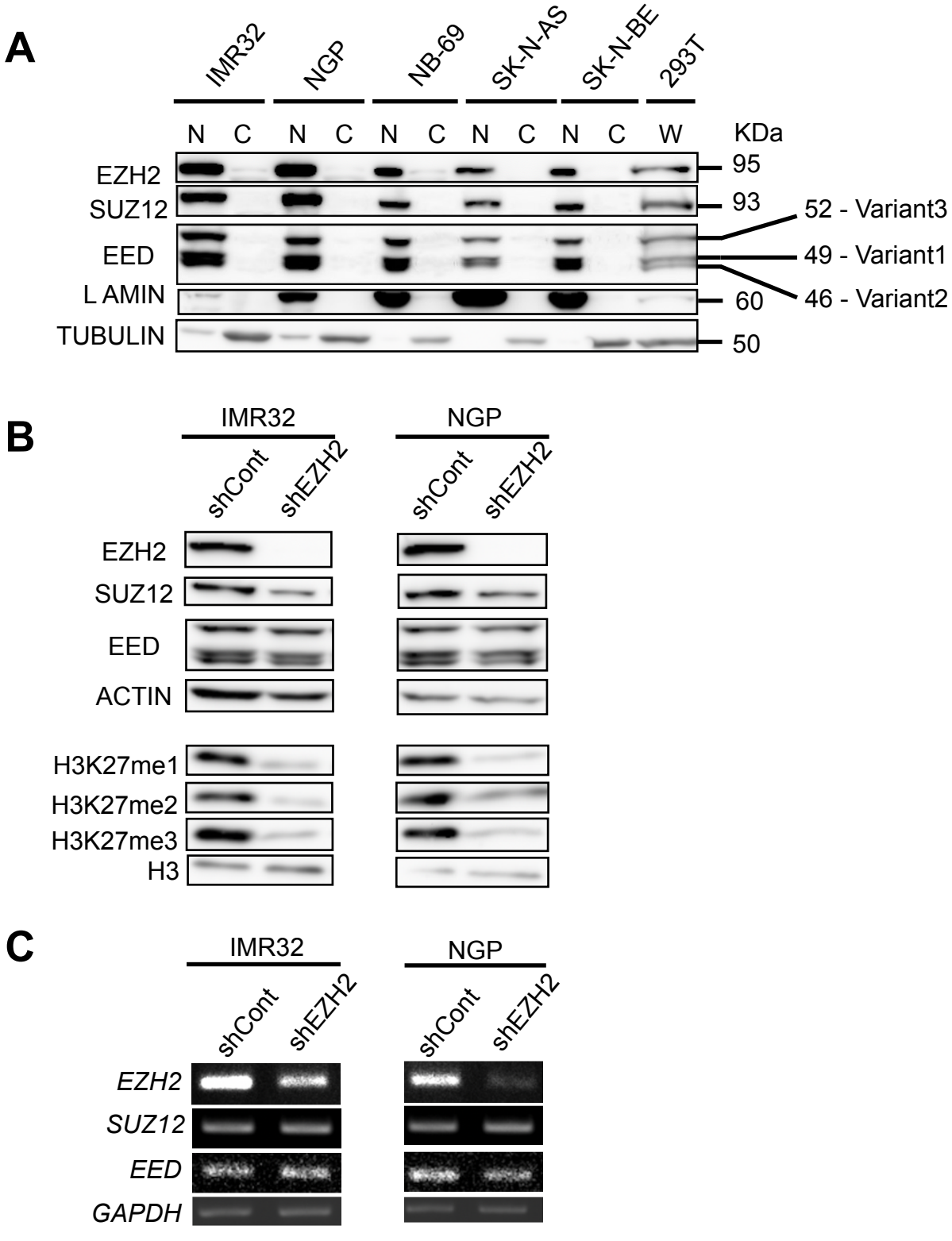

Figure 1. PRC2 core components EZH2, EED, and SUZ12 are mainly localized in nuclear of neuroblastoma cells. **A.** NB cells were fractionated using EMSA buffer (See materials and methods) and EED, EZH2, and SUZ12 were detected by WB. Whole-cell 293T lysate was used as a positive control. **B.** IMR32 and NGP cells were infected with lentivirus with the shCont and shEZH2. EED, EZH2, SUZ12, H3K27me1, H3K27me2, H3K27me3 or total H3 in whole-cell were detected by WB. **C.** mRNA of SUZ12 and EED were checked using RNAs of EZH2 knocked down IMR32 and NGP cells.

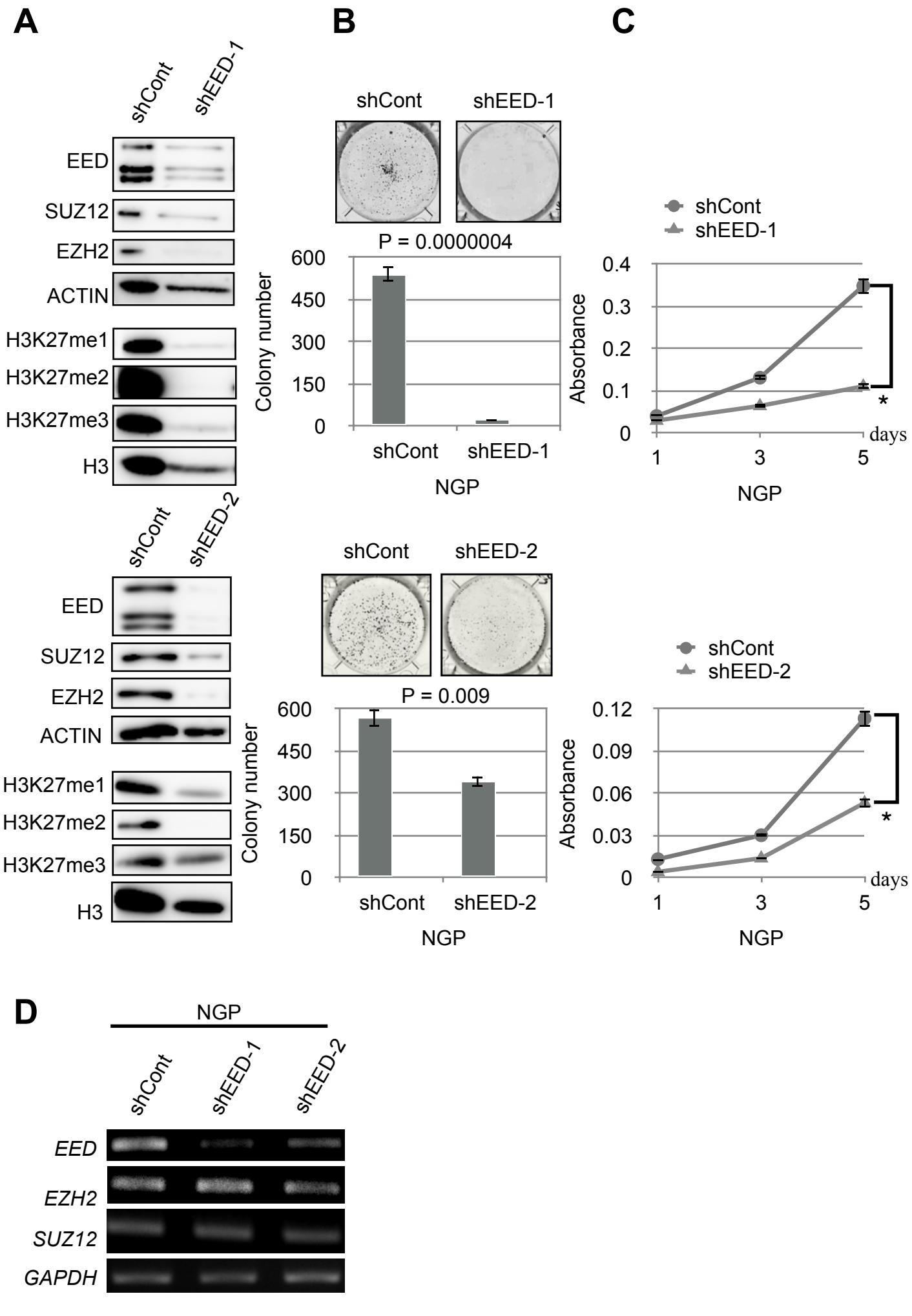
A
shCont
shEED-1
EED
SUZ12
EZH2
ACTIN
H3K27me1
H3K27me2
H3K27me3
H3
shCont
shEED-2
EED
SUZ12
EZH2
ACTIN
H3K27me1
H3K27me2
H3K27me3
H3
B
shCont
shEED-1
P = 0.0000004
Colony number
600
450
300
150
0
shCont
shEED-1
NGP
shCont
shEED-2
P = 0.009
Colony number
600
450
300
150
0
shCont
shEED-2
NGP
C
shCont
shEED-1
Absorbance
0.4
0.3
0.2
0.1
0
*
days
1
3
5
NGP
shCont
shEED-2
Absorbance
0.12
0.09
0.06
0.03
0
*
days
1
3
5
NGP
D
NGP
shCont
shEED-1
shEED-2
EED
EZH2
SUZ12
GAPDH

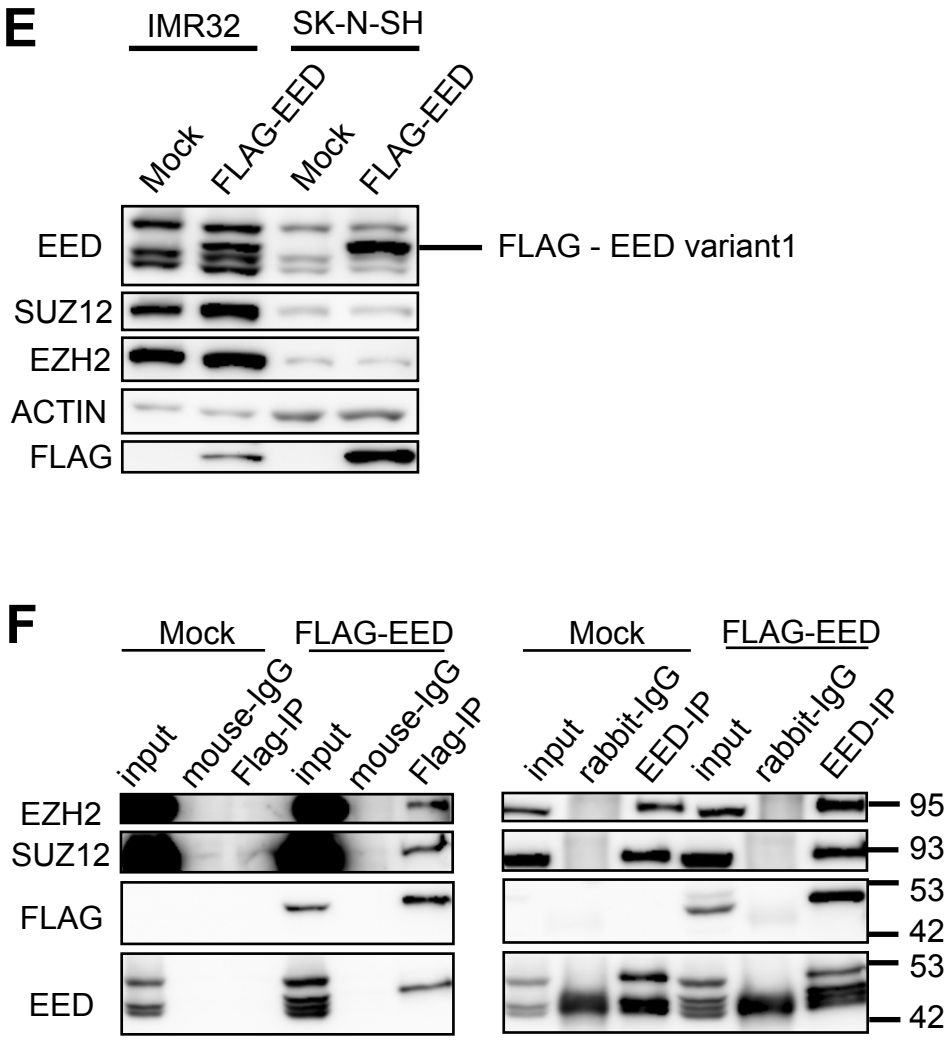

Figure 2. EED knockdown effect on NB cell. NGP cells were infected with lentivirus with shCont, shEED-1 or shEED-2. Cells were collected on day 8 after infection. **A.** The western blotting analysis of EZH2, SUZ12, EED, and H3K27 methylations. **B.** Flat colony formation assay and **C.** cell proliferation assay with WST were performed using shCont, shEED-1, or shEED-2 NGP cells. **D.** mRNA of SUZ12 and EZH2 were checked using RNAs of EED knocked down NGP cells. **E.** Western blotting results demonstrated the bands of EED after EED (variant1) overexpression. **F.** EED and FLAG were immunoprecipitations using EED overexpressed IMR32 cell lysates, and EZH2, SUZ12, FLAG, and EED levels were assessed using western blot analysis.

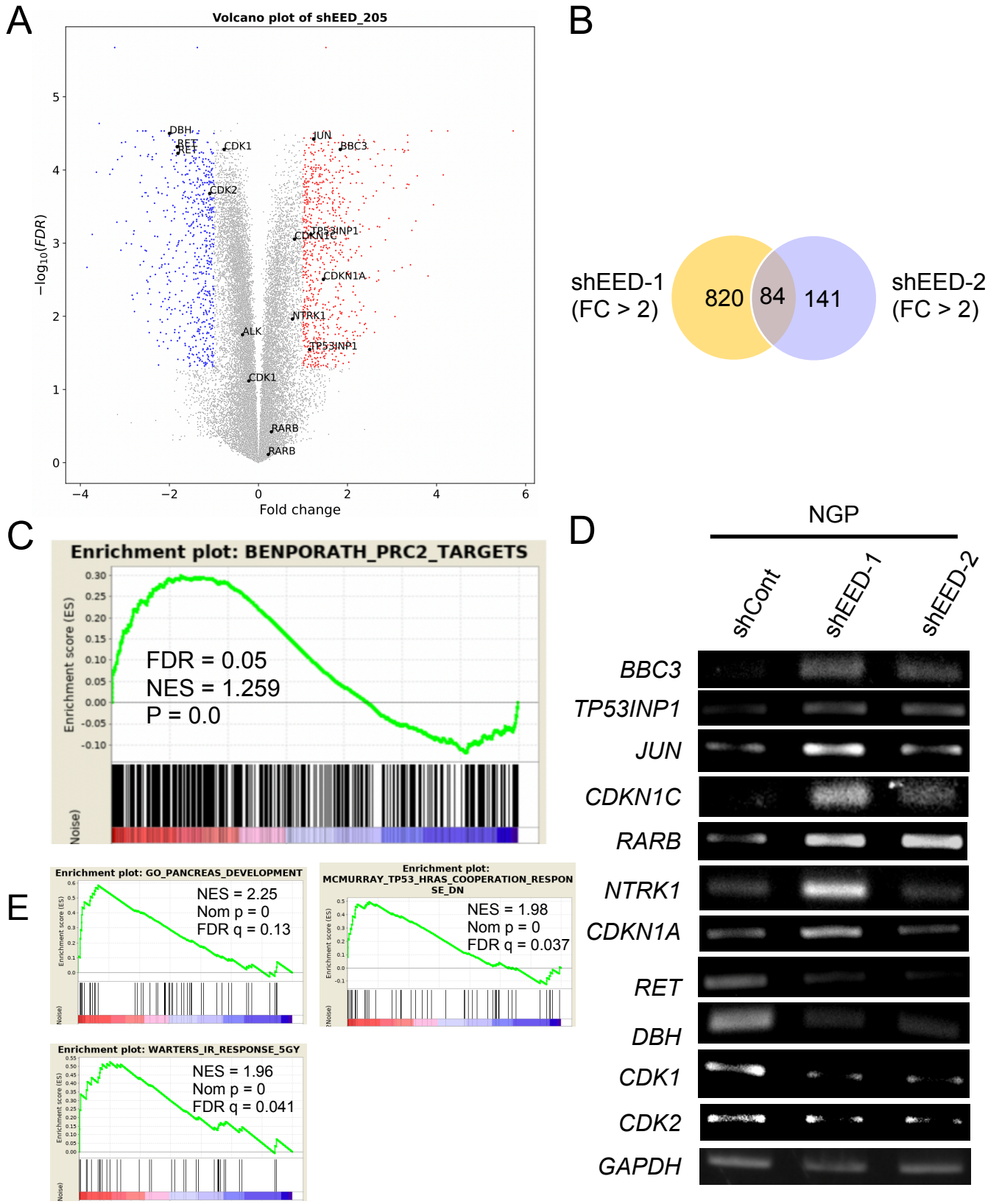

Figure 3. EED is one of the key regulator molecules in NB cell differentiation. **A.** Volcano plot of all genes based on $\log_2$ fold change and FDR values. The colored dot indicated that magnitude of change 2 that is either upregulated (Red) or downregulated (Blue) and statistical significance (FDR<0.05) in shEED-1 compare with shCont treated NGP cells. **B.** Venn diagram showing numbers of upregulated genes after EED knockdown treated with shEED-1 or shEED-2 in NGP cells. Only genes with $\log_2$ fold-change. **C.** Gene set enrichment analysis (GSEA) of microarray data in shEED-1 treated NGP cells display enrichment in PRC2 target genes in BENPORATH-PRC2-TARGETS. **D.** RT-PCR result with genes of interest. **E.** GSEA result of pathway-related genes.

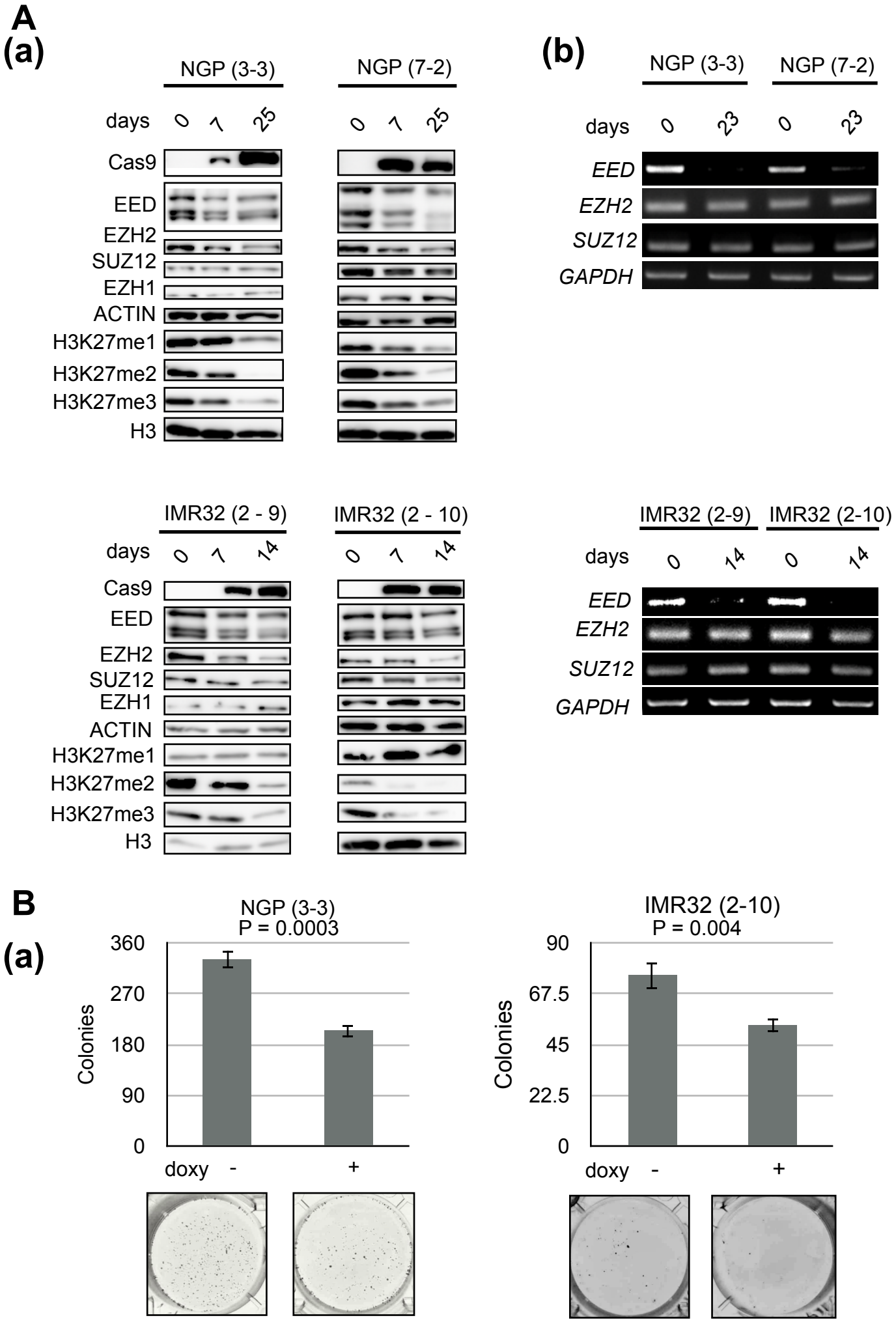
A
(a)
NGP (3-3)
NGP (7-2)
days
0
7
25
Cas9
EED
EZH2
SUZ12
EZH1
ACTIN
H3K27me1
H3K27me2
H3K27me3
H3
IMR32 (2 - 9)
IMR32 (2 - 10)
days
0
7
14
Cas9
EED
EZH2
SUZ12
EZH1
ACTIN
H3K27me1
H3K27me2
H3K27me3
H3
(b)
NGP (3-3)
NGP (7-2)
days
0
23
EED
EZH2
SUZ12
GAPDH
IMR32 (2-9)
IMR32 (2-10)
days
0
14
EED
EZH2
SUZ12
GAPDH
B
(a)
NGP (3-3)
P = 0.0003
Colonies
360
270
180
90
0
doxy
-
+
IMR32 (2-10)
P = 0.004
Colonies
90
67.5
45
22.5
0
doxy
-
+

(b)

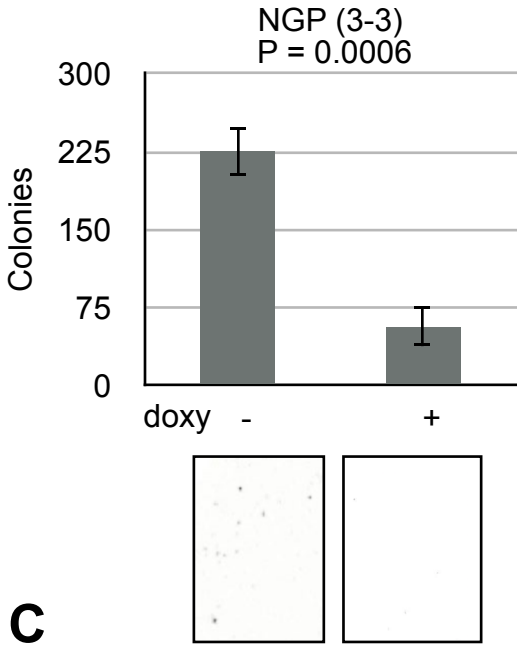
NGP (3-3)
P = 0.0006
Colonies
300
225
150
75
0
doxy - +

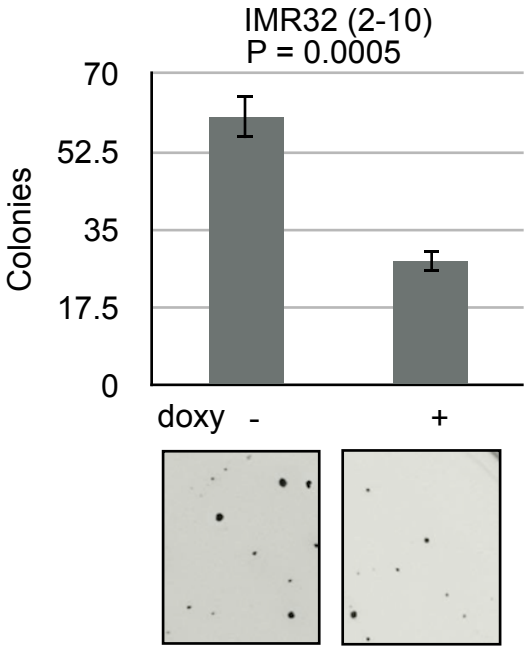
IMR32 (2-10)
P = 0.0005
Colonies
70
52.5
35
17.5
0
doxy - +

C

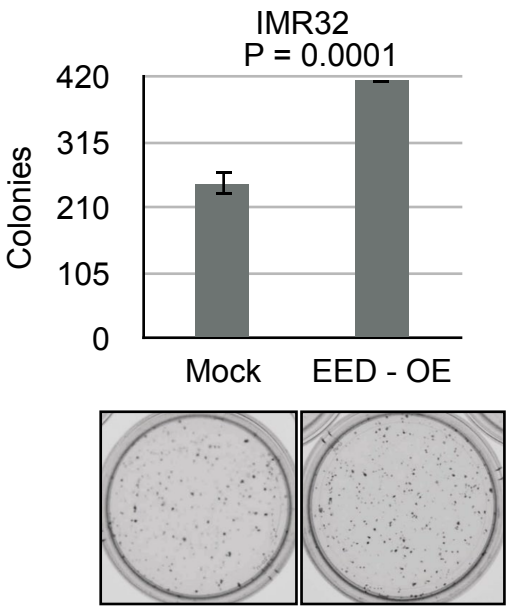
IMR32
P = 0.0001
Colonies
420
315
210
105
0
Mock
EED - OE

D

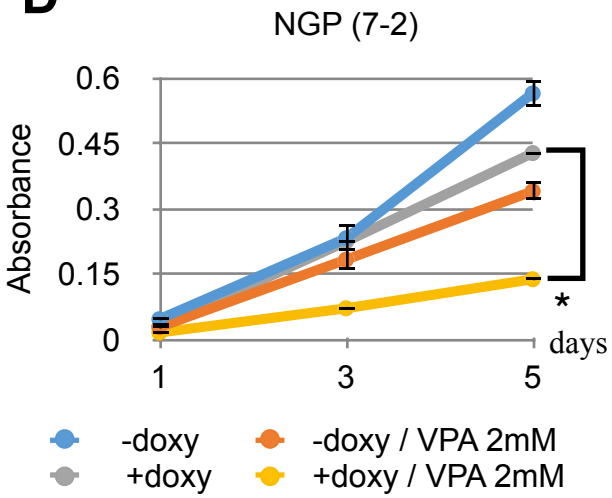
NGP (7-2)
Absorbance
0.6
0.45
0.3
0.15
0
1
3
5
days
*
-doxy
+doxy
-doxy / VPA 2mM
+doxy / VPA 2mM

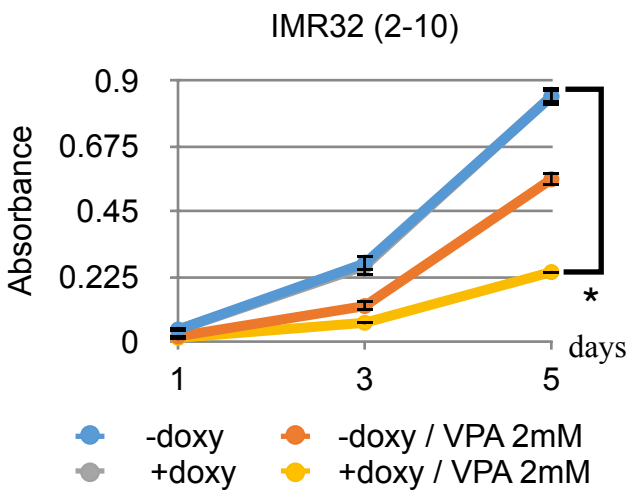
IMR32 (2-10)
Absorbance
0.9
0.675
0.45
0.225
0
1
3
5
days
*
-doxy
+doxy
-doxy / VPA 2mM
+doxy / VPA 2mM

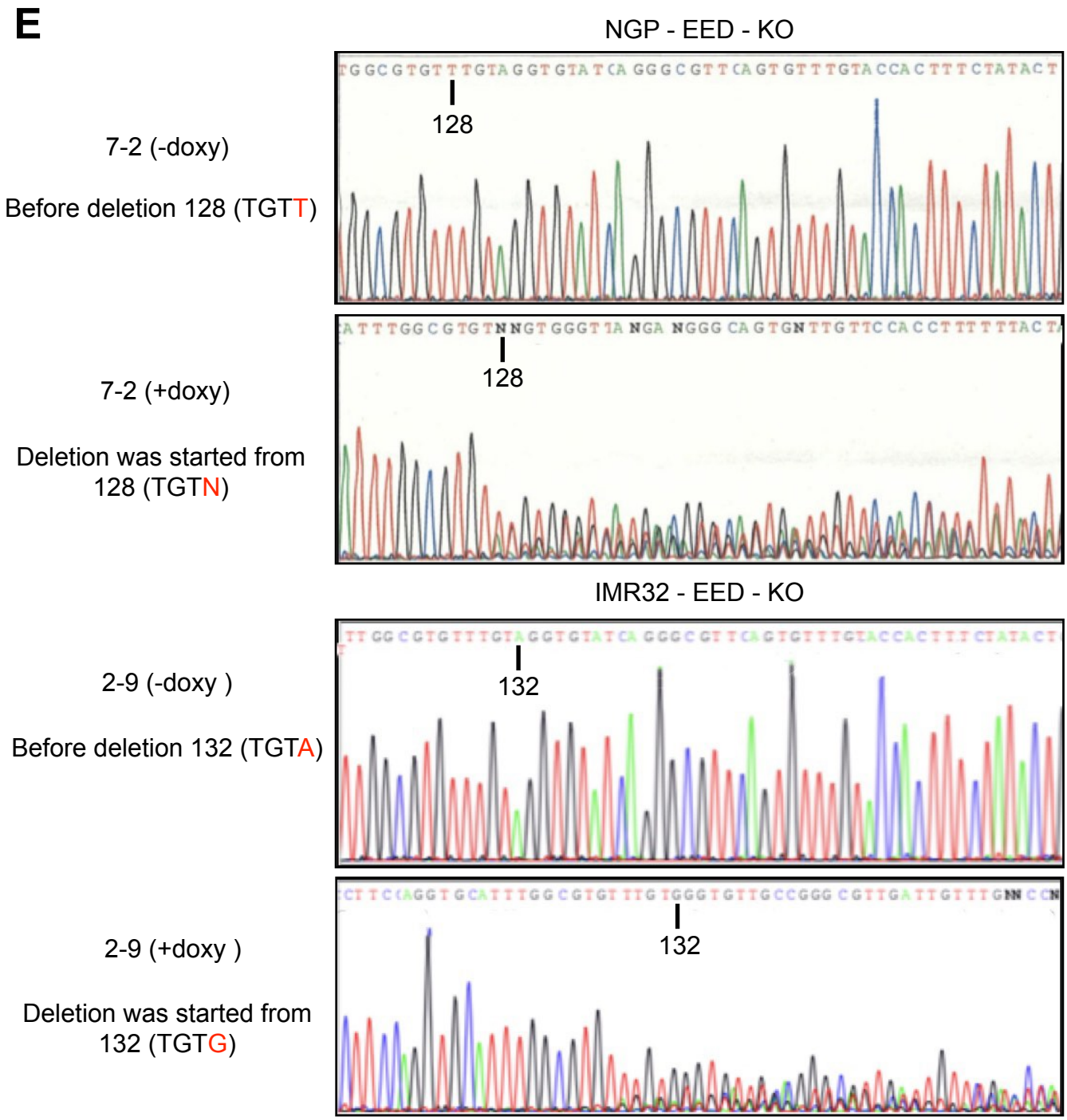

Figure 4. Knockout of EED (EED-KO) from NB cells by CRISPR-Cas9 technique. **A. (a).** Expression levels of the indicated PRC2 components, EZH2, SUZ12, or EED, and H3K27 methylations were detected by WB. EED-KO NGP 3-3 and 7-2 cells were collected after adding doxycycline for 7 and 25 days, EED knocked out IMR32 2-9, and 2-10 cells were collected after adding doxycycline 7 and 14 days. **(b).** RT-PCR results of EED, EZH2 and SUZ12 using EED knocked out NGP and IMR32 cells. **B. (a).** Flat colony formation assay and **(b).** soft agar colony formation assays were performed using EED knocked out NGP (3-3) and IMR32 (2-9) cells. - doxycycline cell represents EED knocked out cell and + doxycycline cell represents EED did not knocked out cell. Full names of cells were annotated in the result part. **C.** Soft agar colony formation assay, mock and EED-OE cells stained colonies after an incubation period of 12 and 25 days. **D.** Cell proliferation assay was performed by WST after treating the EED knocked out NGP (7-2) and IMR32 (2-10) cells with 2 mM valproicacid for 5 days. **E.** Genomic sequencing result of NGP-EED-KO and IMR32-EED-KO cells.

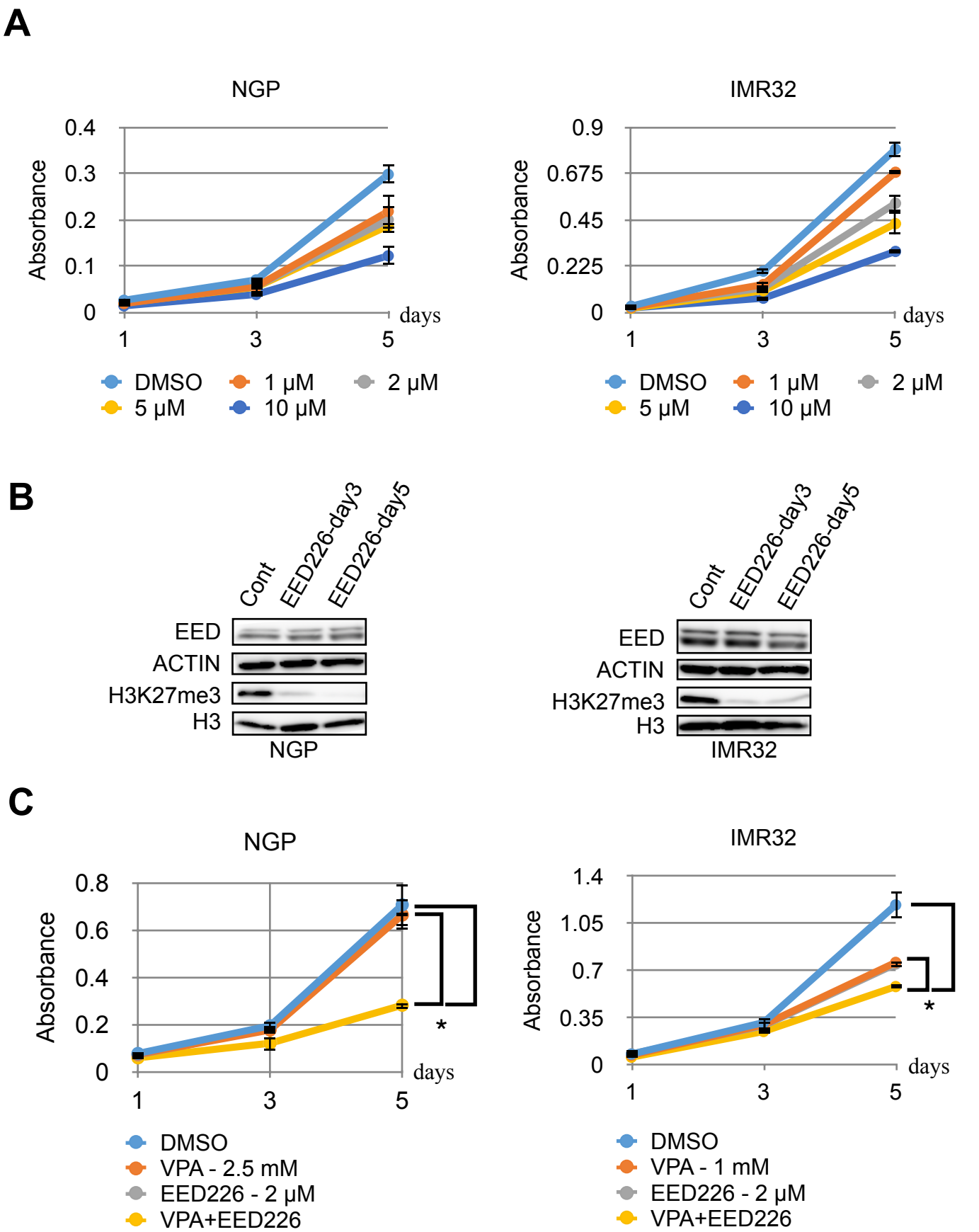
A
NGP
Absorbance
0.4
0.3
0.2
0.1
0
1
3
5
days
DMSO
1 μM
2 μM
5 μM
10 μM
IMR32
0.9
0.675
0.45
0.225
B
Cont
EED226-day3
EED226-day5
EED
ACTIN
H3K27me3
H3
C
0.8
0.6
1.4
1.05
0.7
0.35
*
VPA - 2.5 mM
VPA - 1 mM
EED226 - 2 μM
VPA+EED226

D

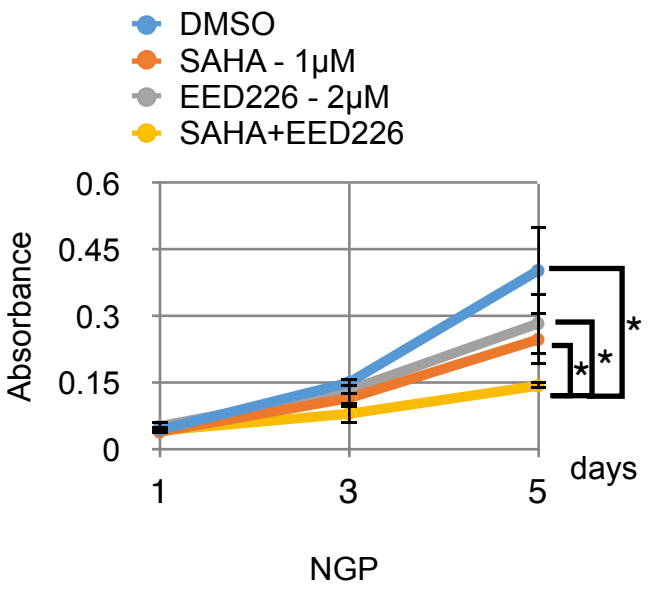
DMSO
SAHA - 1μM
EED226 - 2μM
SAHA+EED226
Absorbance
0.6
0.45
0.3
0.15
0
1
3
5
days
*
*
*
NGP

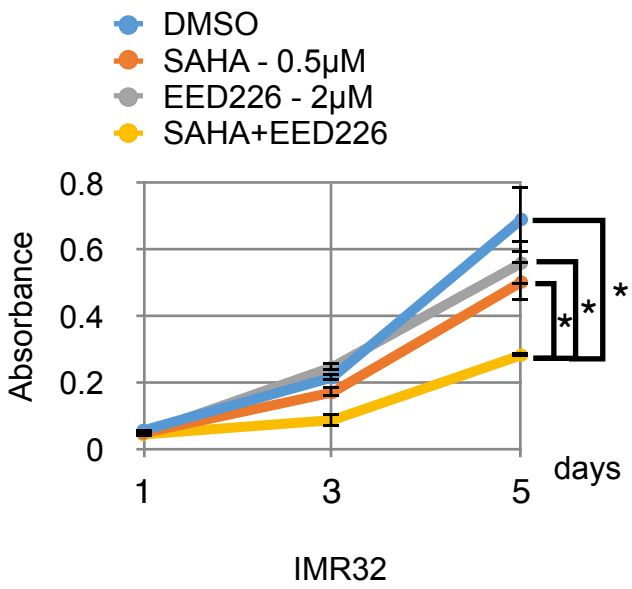
DMSO
SAHA - 0.5μM
EED226 - 2μM
SAHA+EED226
Absorbance
0.8
0.6
0.4
0.2
0
1
3
5
days
*
*
*
IMR32

E

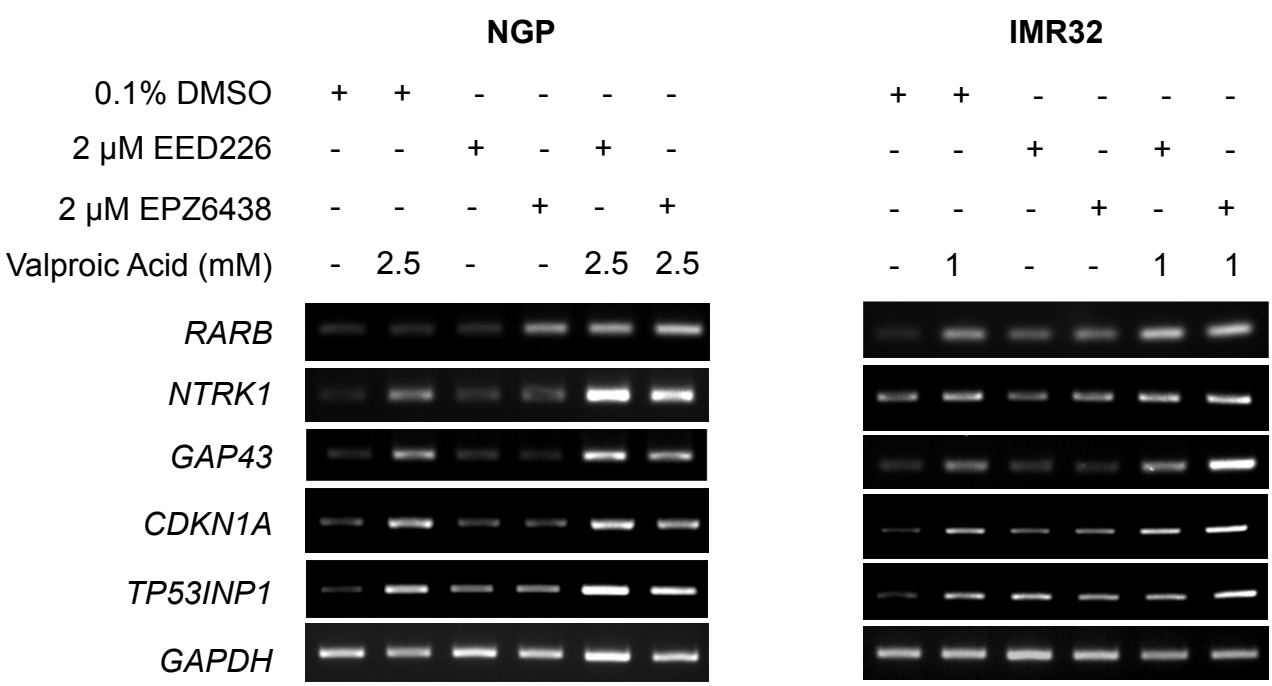
NGP
IMR32
0.1% DMSO
2 μM EED226
2 μM EPZ6438
Valproic Acid (mM)
+ + - - - -
- - + - + -
- - - + - +
- 2.5 - - 2.5 2.5
+ + - - - -
- - + - + -
- - - + - +
- 1 - - 1 1
RARB
NTRK1
GAP43
CDKN1A
TP53INP1
GAPDH

F

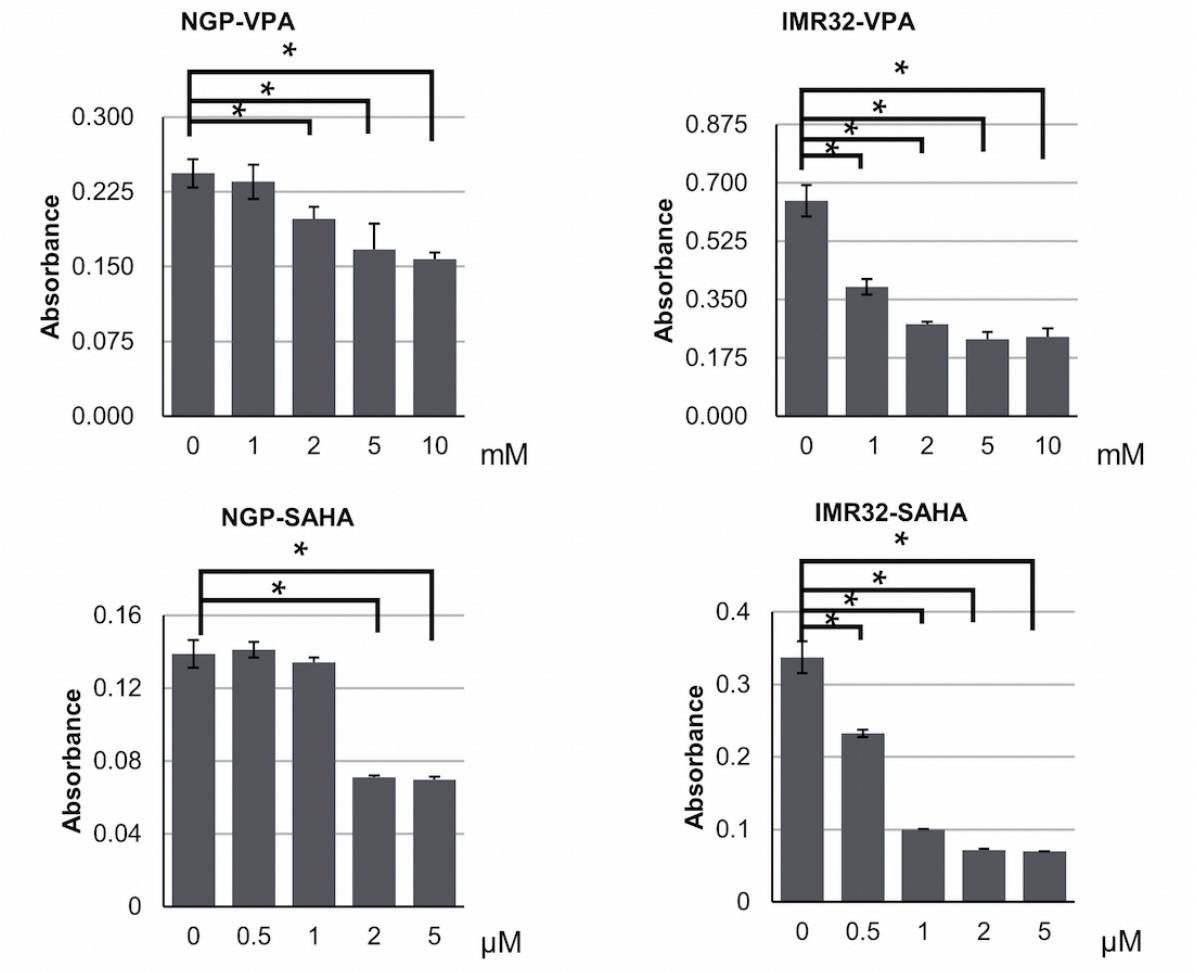
NGP-VPA
Absorbance
0.300
0.225
0.150
0.075
0.000
0 1 2 5 10
mM
IMR32-VPA
Absorbance
0.875
0.700
0.525
0.350
0.175
0.000
0 1 2 5 10
mM
NGP-SAHA
Absorbance
0.16
0.12
0.08
0.04
0
0 0.5 1 2 5
μM
IMR32-SAHA
Absorbance
0.4
0.3
0.2
0.1
0
0 0.5 1 2 5
μM

G

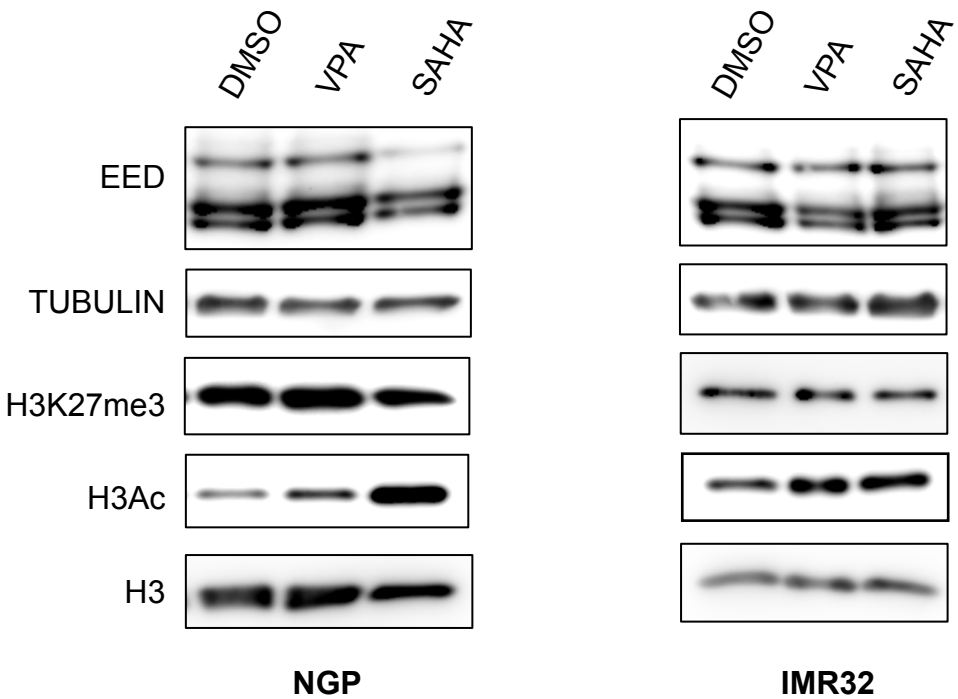
DMSO
VPA
SAHA
EED
TUBULIN
H3K27me3
H3Ac
H3
NGP
DMSO
VPA
SAHA
IMR32

H

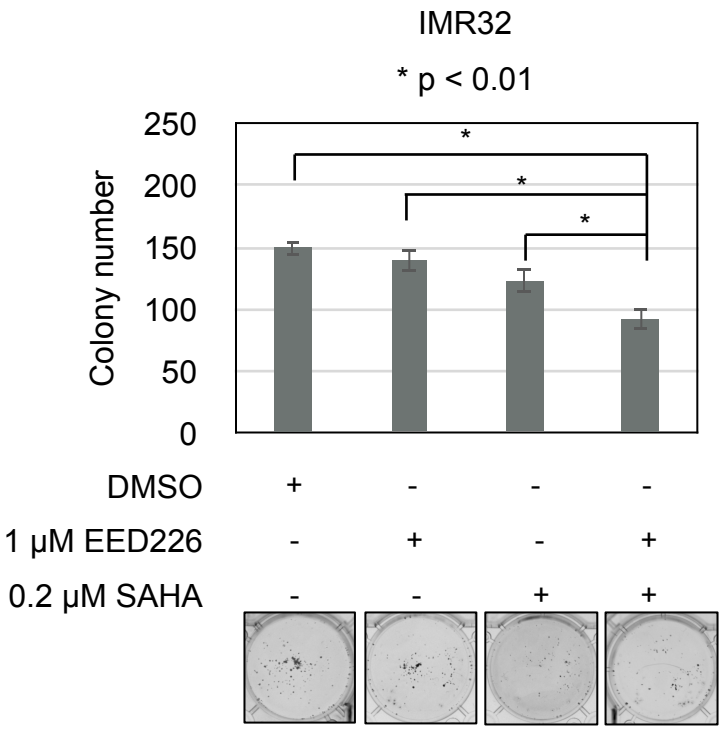
IMR32
* p < 0.01
Colony number
250
200
150
100
50
0
*
*
*
DMSO + - - -
1 μM EED226 - + - +
0.2 μM SAHA - - + +

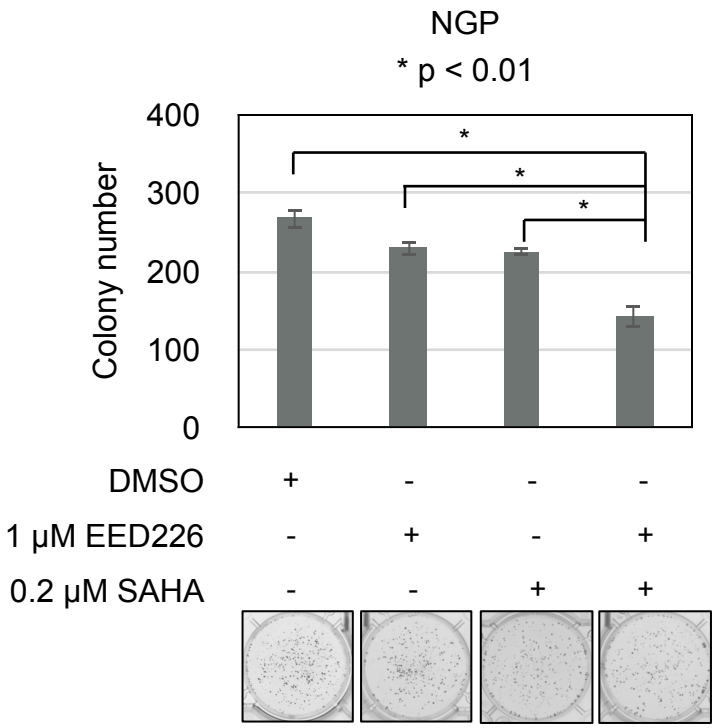
NGP
* p < 0.01
Colony number
400
300
200
100
0
*
*
*
DMSO + - - -
1 μM EED226 - + - +
0.2 μM SAHA - - + +

I

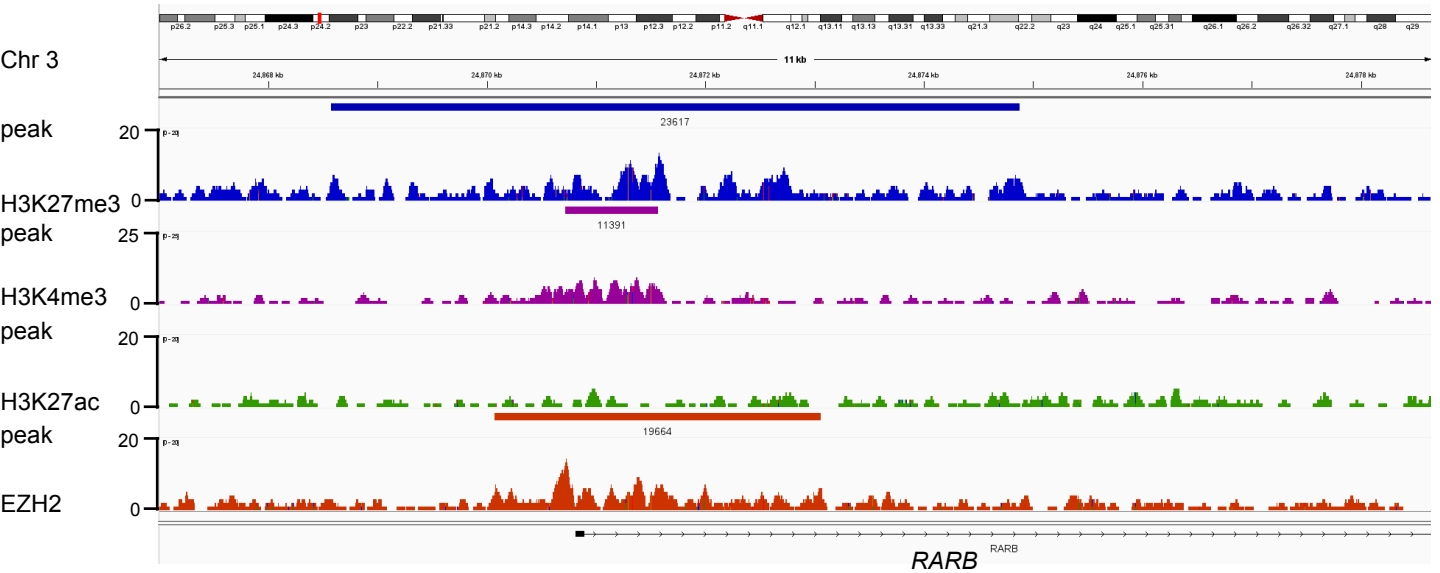
Chr 3
peak
H3K27me3
peak
H3K4me3
peak
H3K27ac
peak
EZH2
23617
11391
19664
RARB
RARB

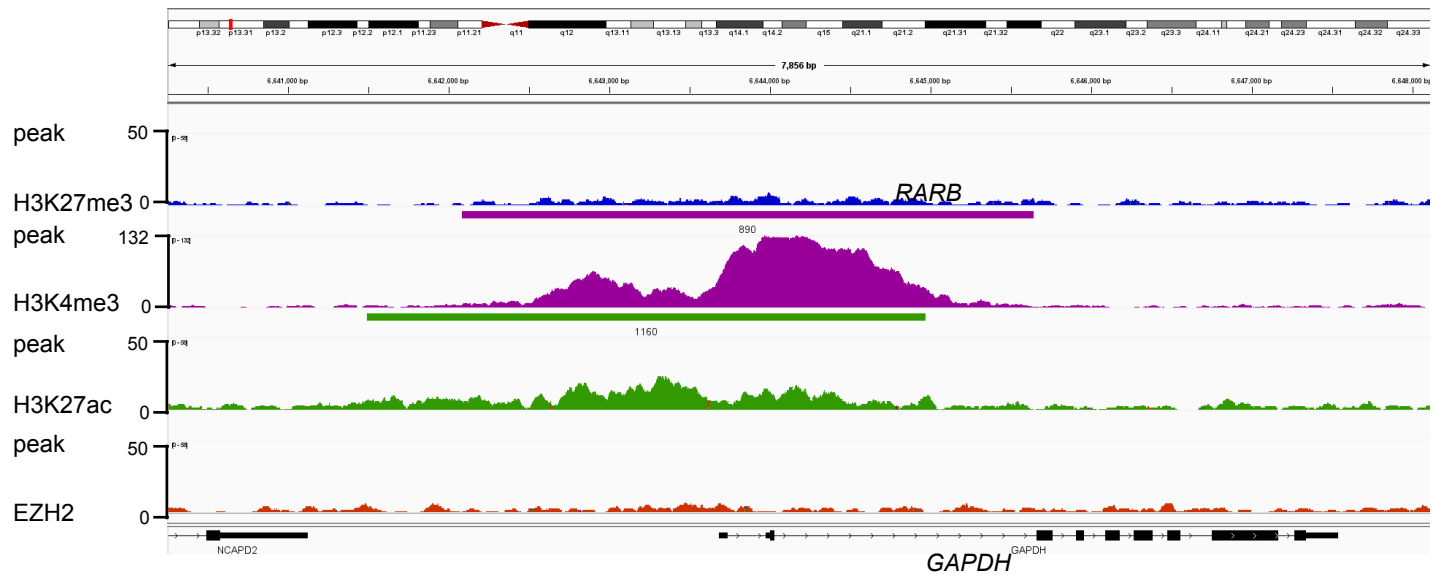
peak
H3K27me3
peak
H3K4me3
peak
H3K27ac
peak
EZH2
RARB
890
1160
NCAPD2
GAPDH
GAPDH

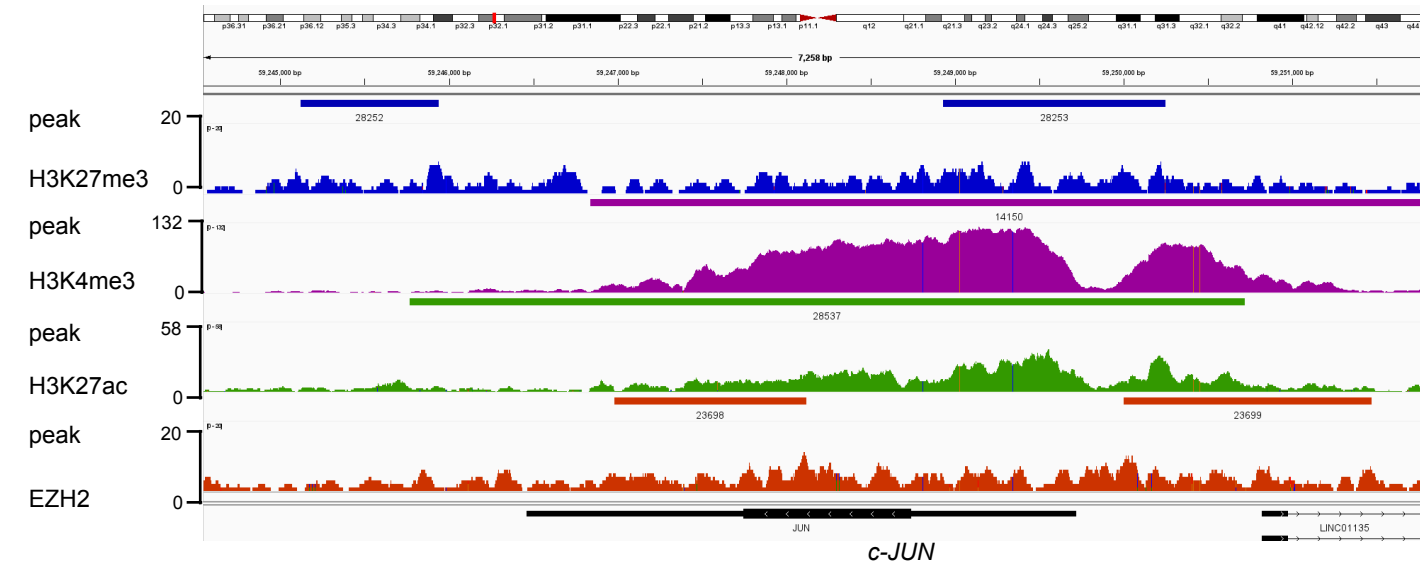
peak
H3K27me3
peak
H3K4me3
peak
H3K27ac
peak
EZH2
20
0
132
0
58
0
20
0
28252
28253
14150
28537
23698
23699
JUN
LINC01135

c-JUN

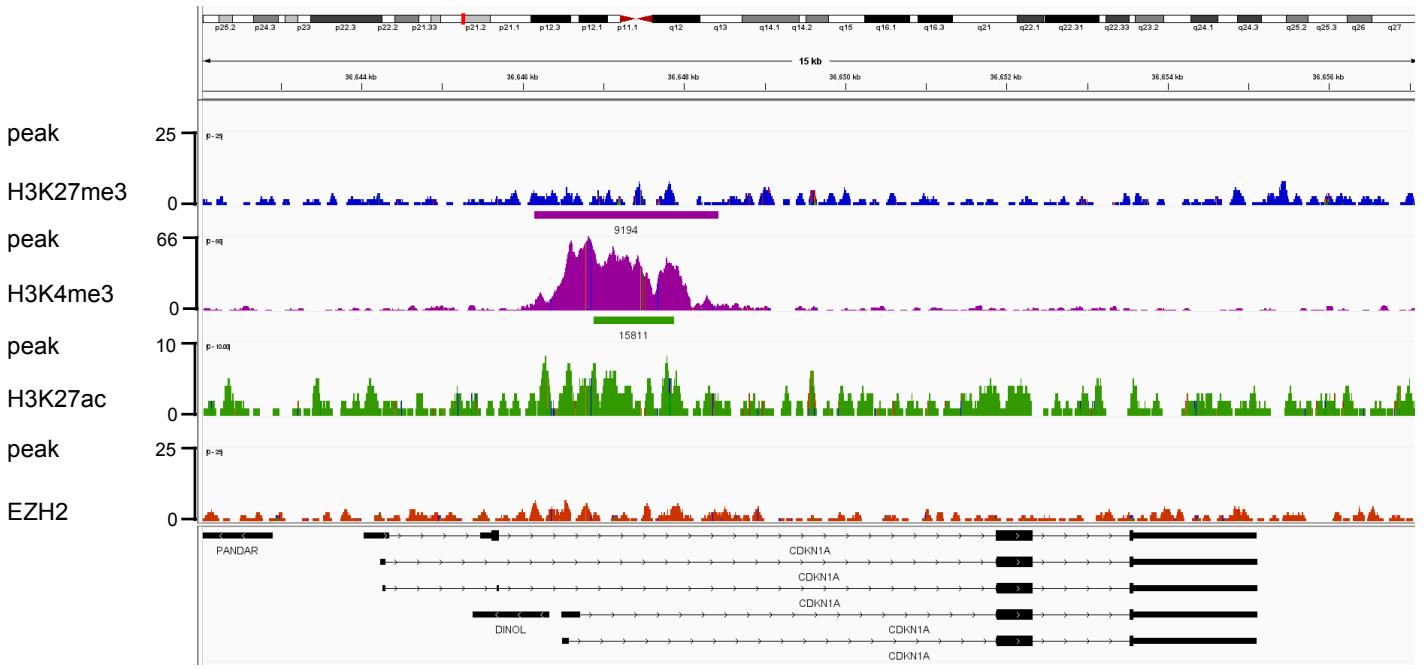
peak
H3K27me3
peak
H3K4me3
peak
H3K27ac
peak
EZH2
25
0
66
0
10
0
25
0
9194
15811
PANDAR
CDKN1A
CDKN1A
CDKN1A
DINOL
CDKN1A
CDKN1A

CDKN1C

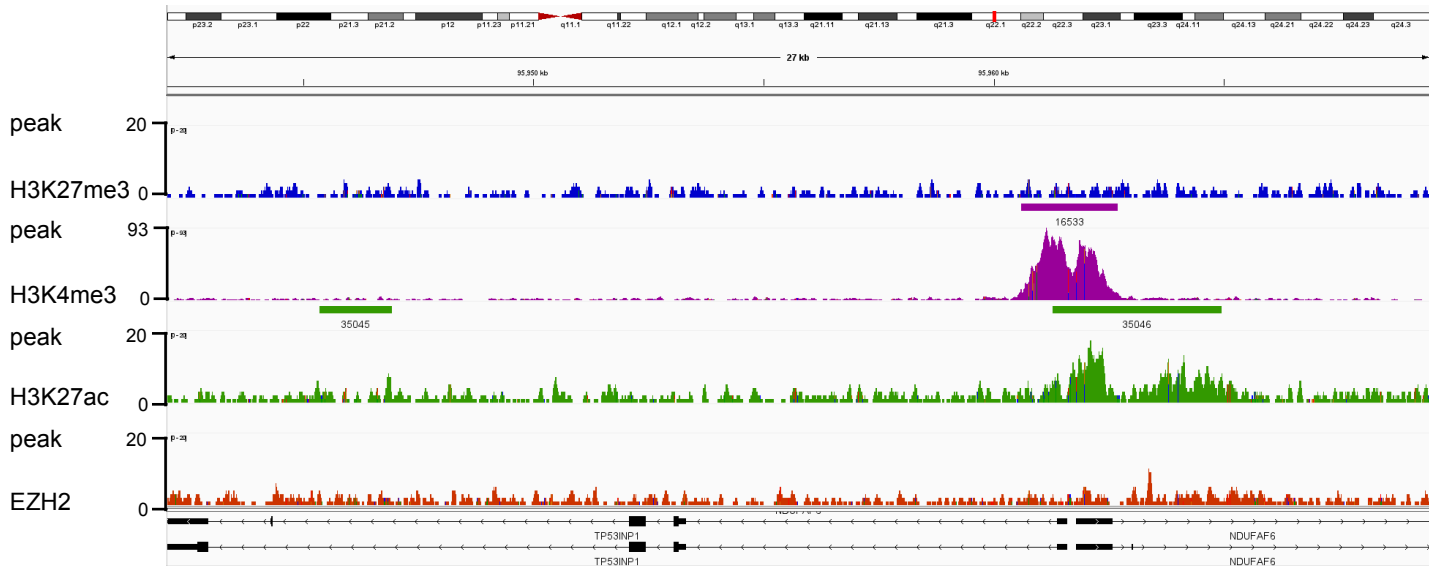

TP53INP1

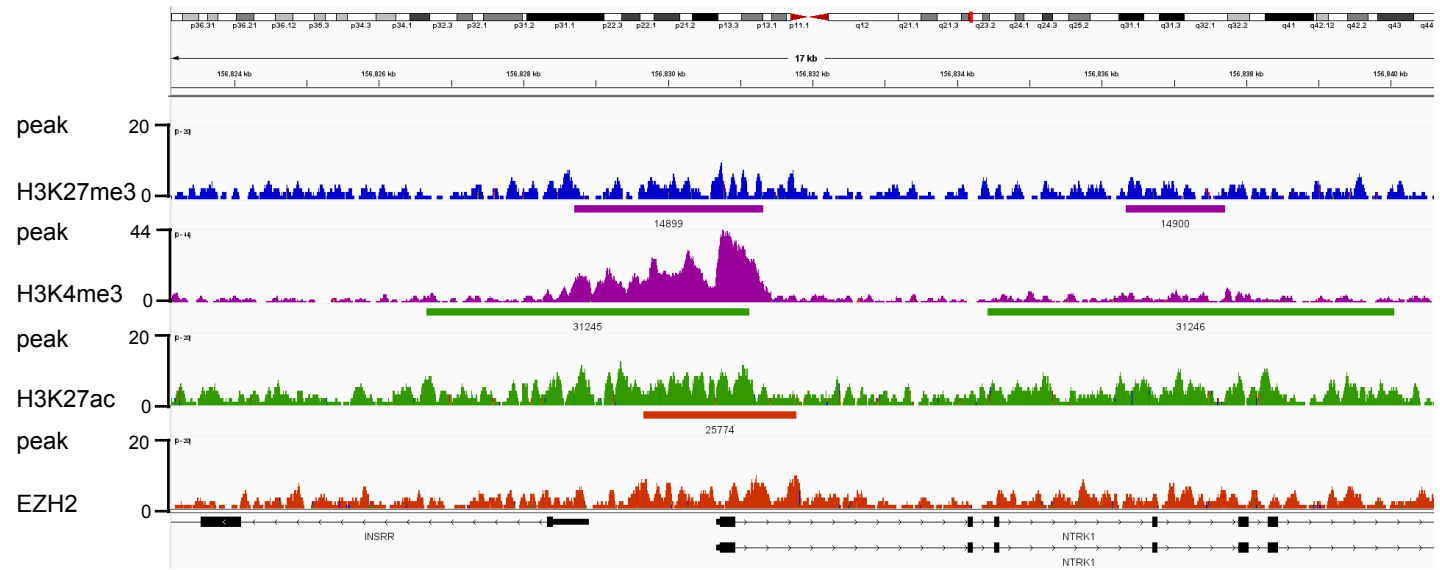

NTRK1

Figure 5. EED inhibitor and VPA have a synergistic effect on inhibiting the NB cell proliferation. **A.** Cell proliferation assay with WST solution of NGP and IMR32 cells after being treated with EED226 (0, 1, 2, 5, 10 μM) for 5 days. **B.** Western blot results for EED and H3K27me3 of NGP and IMR32 cells after being treated with EED226 (2 μM) for 5 days. **C.** Cell proliferation assay with WST solution of NGP and IMR32 cells after treated with EED226 (2 μM) alone, VPA (2.5, 1 mM) alone, or a combination of EED226 with VPA for 5 days. **D.** The effects of EED226 and/or suberanilohydroxamic acid (SAHA) were assessed by the WST-8 cell proliferation assay. NGP and IMR32 cells were treated with EED226 (2 μM) alone, SAHA (1 μM: NGP; 0.5 μM: IMR32) alone, or the combination of EED226/SAHA for 5 days. **E.** IMR32 and NGP cells were treated for 3 days with VPA and/or, EED-226 and EPZ6438 at the indicated concentration. Semi-quantitative RT-PCR was performed for PRC2 targets, differentiation markers, and cell cycle repressor genes. **F.** NGP and IMR32 cells were treated with VPA or SAHA for 3 days. VPA or SAHA were added to NGP and IMR32 cells and cell viability was determined by WST-8 cell proliferation assay. The IC50 value of VPA was 7.98 mM in NGP and 1.55 mM in IMR32 cells, And SAHA was in NGP 1.52 μM, in IMR32 0.59 μM (Table 8). The significance of differences was assessed by the unpaired two-tailed Student's t-test (*: $P < 0.05$). **G.** Western blotting results of VPA or SAHA-treated NGP and IMR32 cells. Cells were treated with VPA with 2.5 mM in NGP and 1 mM in IMR32 for 96 hours. And SAHA treatments were performed at 1 μM in NGP and 0.5 μM in IMR32 for 96 hours. **H.** Flat colony assay with EED226 and SAHA. Cells were seeded on 6-well plates (day 0) and inhibitors were added at the indicated concentrations (day 1). Cells were fixed and stained on day 8 (IMR32) and day 13 (NGP). **I.** IGV (integrative genomic viewer) image of H3K27me3, H3K4me3, H3K27ac, and EZH2 of *RARB*, *GAPDH, c-JUN*, *CDKN1C*, *TP53INP1*, *NTRK1* around transcription start sites in IMR32 cells. ChIP-sequencing experiments were performed in our previous study (Endo Y et al., manuscript in preparation, GSE162059). Peak calls were performed by the DANPOS algorithm using default settings. The y-axis of histograms shows the actual read count.

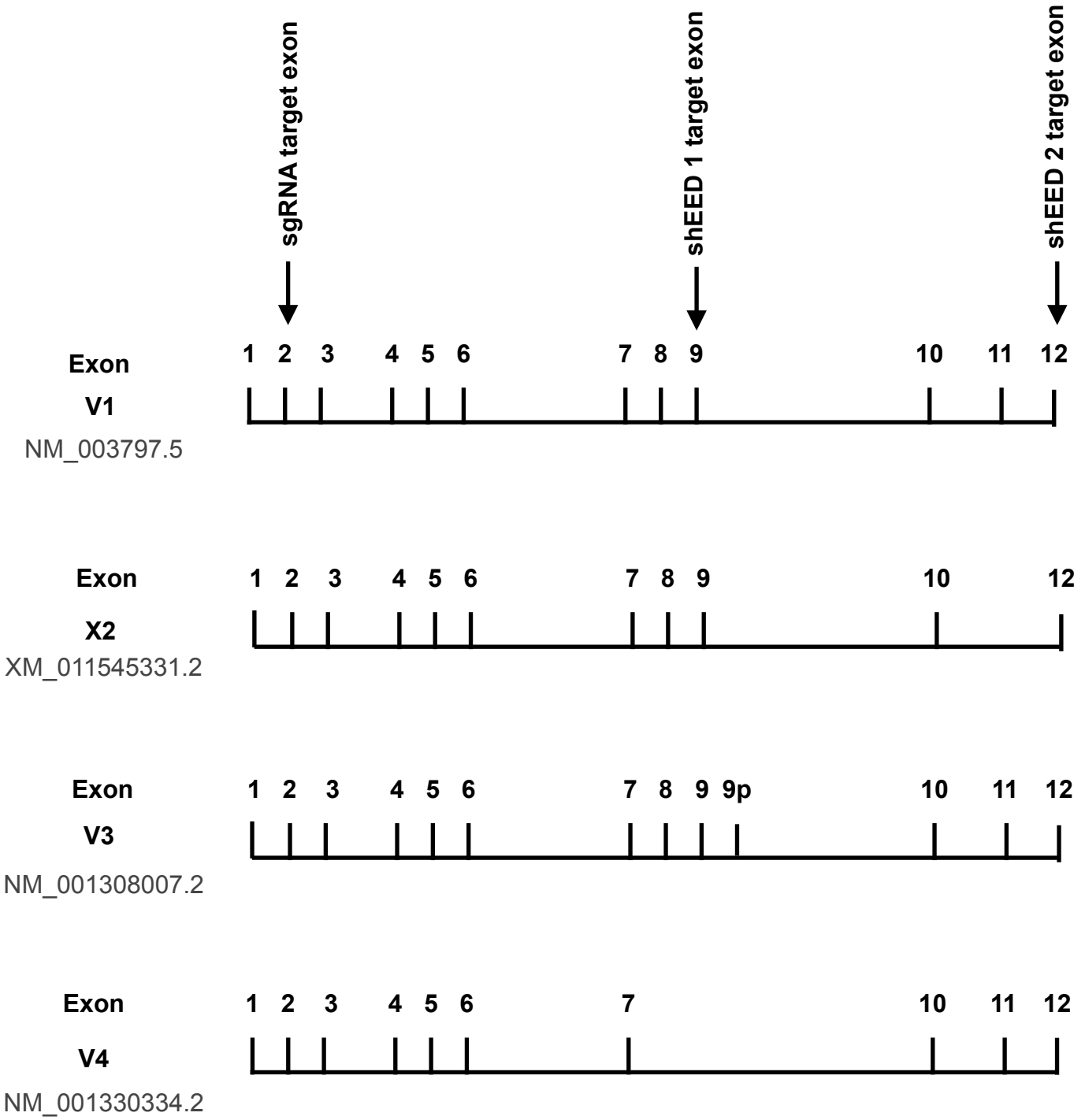

The EED Monoclonal antibody is produced by immunizing animals with a synthetic peptide corresponding to residues near the amino terminus of human EED protein.

Figure 6. A monoclonal antibody is produced by immunizing animals with a synthetic peptide corresponding to residues near the amino terminus of the human EED protein. The arrows indicate the knocked out exon by sgRNAs and the knocked down exons by the indicated shRNAs.

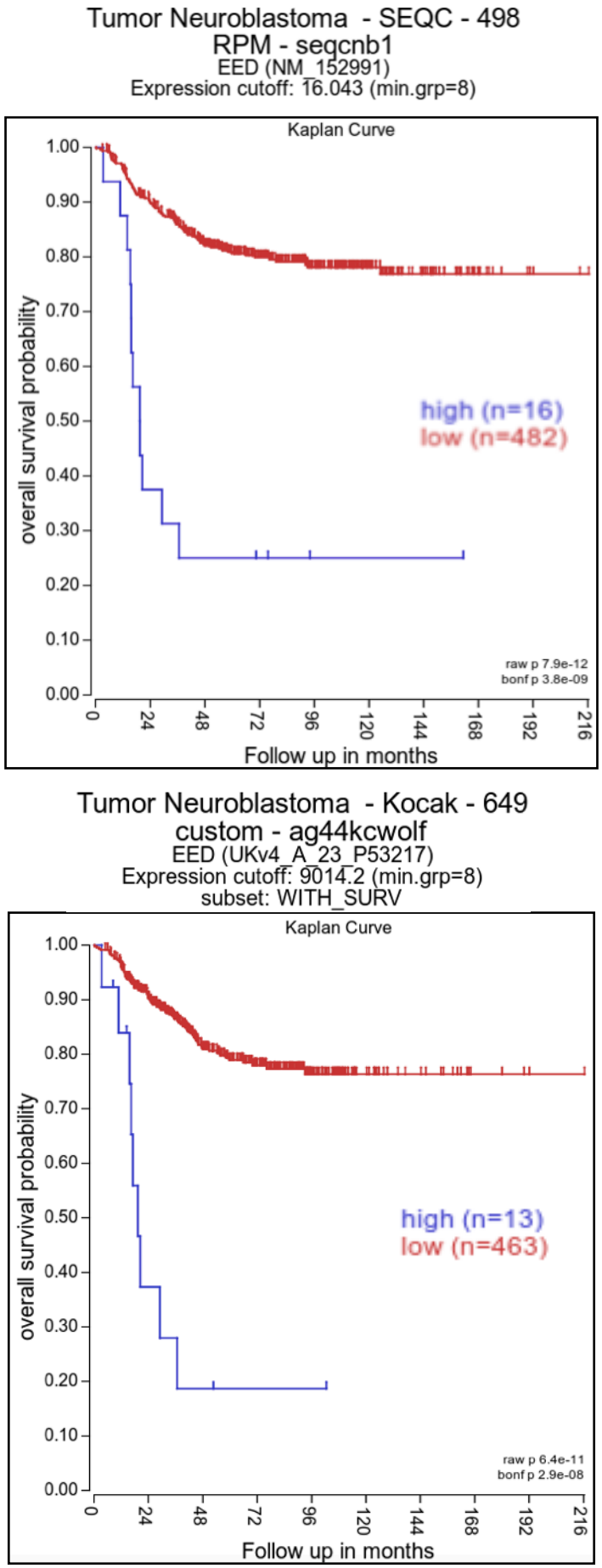

Figure 7. Information of Tumor Neuroblastoma - SEQC - 498, Tumor Neuroblastoma - kocak - 649 overall survival probability**.**

Table 1. Primary antibodies for western blotting

Target protein	First antibody
EED	Anti EED rabbit (E4L6E Cell Signaling)
EZH2	Anti EZH2 rabbit polyclonal (07-689 Millipore)
SUZ12	Anti SUZ12 rabbit polyclonal (ab12073 abcam)
EZH1	Anti EZH1 rabbit polyclonal (ABE281 Millipore)
ACTIN	Anti α-actin rabbit polyclonal (20-33 Sigma)
TUBULIN	Anti β-tubulin mouse monoclonal (Boehringer)
LAMIN	MAB3211 JOL2 Chemicon
H3	Anti Histone H3 rabbit polyclonal (ab1791 Millipore)
H3K27me1	Anti H3k27me1 mouse monoclonal (07-449 active motif - ABI 0821)
H3K27me2	Anti H3k27me2 rabbit monoclonal (CST, D18C8)
H3K27me3	Anti H3k27me3 rabbit polyclonal (07-449 Millipore)
Cas9	Anti Cas9 mouse mAb (7A9-3A3 Cell Signaling)
H3Ac	H3Ac Anti H3Ac rabbit polyclonal (06-599 Millipore)

Table 2. RT-PCR primers

Name	Sequence (5'-3')	Location
EED (F)	GAGAGGGAAGTGTCGACTGC	Exon4
EED (R)	CATTTTCCCTTTCCCCAACT	Exon6
SUZ12 (F)	TGCAGTTCACTCTTCGTTGG	Exon8
SUZ12 (R)	TGCTTCAGTTTGTTGCCTTG	Exon10
EZH2 (F)	TCTATTGCTGGCACCATCTG	Exon16
EZH2 (R)	TGCATCCACCACAAAATCAT	Exon18
EED-sgRNA	GGTGCATTTGGCGTGTTTGT	Exon2
BBC3 (F)	GTCCTCAGCCCTCGCTCT	Exon3
BBC3 (R)	CTGCTGCTCCTCTTGTCTCC	Exon4
RET (F)	TGTGGAGACCCAAGACATCA	Exon6
RET (R)	CCGAGACGATGAAGGAGAAG	Exon8
CDKN1C (F)	GCCTCTGATCTCCGATTTCTTC	Exon1
CDKN1C (R)	CATCGCCCGACGACTTCT	Exon2
JUN (F)	CCCCAAGATCCTGAAACAGA	Exon1
JUN (R)	CCGTTGCTGGACTGGATTAT	Exon1
TP53INP1 (F)	GGCCCACGTACAATGACTCT	Exon2
TP53INP1 (R)	GATGCCGGTAAACAGGAAAA	Exon3
DBH (F)	GCCATCCATTTCCAGCTCCT	Exon1
DBH (R)	TCCAGGCGTCCGCAAAATAG	Exon2
NTRK1 (F)	TCAACAAATGTGGACGGAGA	Exon10
NTRK1 (R)	GTGGTGAACACAGGCATCAC	Exon11~12
RARB (F)	GAAAAAGACGACCCAGCAAG	Exon6
RARB (R)	ATGAGAGGTGGCATTGATCC	Exon8
CDK1 (F)	TTTTCAGAGCTTTGGGCACT	Exon6~7
CDK1 (R)	CCATTTTGCCAGAAATTCGT	Exon8
CDK2 (F)	TGTACCTCCCCTGGATGAAG	Exon6
CDK2 (R)	TGAGTCCAAATAGCCCAAGG	Exon7
CDKN1A (F)	GACACCACTGGAGGGTGACT	Exon2
CDKN1A (R)	GGCGTTTGGAGTGGTAGAAA	Exon3
hGAP43 (F)	GGAGAAGGCACCACTACTGC	Exon3
hGAP43 (R)	GGCGAGTTATCAGTGGAAGC	Exon3

Table 3. hEED shRNA (Sigma Mission)

Name	Location	Sequence	Clone ID
TRCN0000021206	Exon12	CCGGGCAGCATTCTTATAGCTGTTTCTCGAGAAACAGCTATAAGAATGCTGCTTTTT	NM_003797.2-1722s1c1
TRCN0000021205	Exon9	CCGGCCAGAGACATACATAGGAATTCTCGAGAATTCCTATGTATGTCTCTGGTTTTT	NM_003797.2-1359s1c1

Table 4. EED - variants

NCBI number	EED	Sequence	Amino acid number	Estimated molecular weight
NM_003797.5	Variant1	1326bp	441	49KDa
XM_011545331.2	Variant X2	1247bp	412	46KDa
NM_001308007.2	Variant3	1400bp	466	52KDa
NM_001330334.2	Variant4	1085bp	371	41KDa

Table 5. De-repressed genes by shEED-1 and shEED-2

Supplement table 5							
Commonly de-repressed 84 genes (FC > 2) in EED knockdown using sh205 and sh206 in NGP cells.							
ProbeName	FC ([02_shEED205] Vs [01_sh_con]) of UP - FC ([02_shEED205] Vs [01_sh_con]) (Entity list of selection)	p (Corr) ([02_shEED205] Vs [01_sh_con])	FC ([03_shEED206] Vs [01_sh_con]) of UP - FC ([03_shEED206] Vs [01_sh_con]) (Entity list of selection)	p (Corr) ([03_shEED206] Vs [01_sh_con])	Regulation ([03_shEED206] Vs [01_sh_con]) of UP - FC ([03_shEED206] Vs [01_sh_con]) (Entity list of selection)	GeneSymbol	Description
A_23_P11543	5.1767235	1.64E-04	2.836332	0.002192965	up	FUCA1	Homo sapiens fucosidase, alpha-L- 1, tissue (FUCA1), mRNA [NM_000147]
A_21_P0012249	2.060912	0.04599114	3.2689674	0.010413752	up		
A_33_P3347707	3.4755268	4.58E-05	2.0753126	4.52E-04	up	NOVA2	Homo sapiens neuro-oncological ventral antigen 2 (NOVA2), mRNA [NM_002516]
A_23_P166616	5.338886	0.0019404496	3.6897585	0.008378139	up	AGTR1	Homo sapiens angiotensin II receptor, type 1 (AGTR1), transcript variant 4, mRNA [NM_031850]
A_23_P121795	3.1616113	0.0019132901	2.0959418	0.030617256	up	SORBS2	Homo sapiens sorbin and SH3 domain containing 2 (SORBS2), transcript variant 2, mRNA [NM_021069]
A_33_P3274935	10.661183	0.001160399	3.8809743	0.021716908	up	HID1	Homo sapiens HID1 domain containing (HID1), mRNA [NM_030630]
A_33_P3387691	4.6033525	7.87E-04	3.2465668	0.007857147	up	SCML4	Homo sapiens sex comb on midleg-like 4 (Drosophila) (SCML4), transcript variant 1, mRNA [NM_198081]
A_23_P101392	3.04335	4.68E-04	2.1217973	0.005156988	up	TMEM38A	Homo sapiens transmembrane protein 38A (TMEM38A), mRNA [NM_024074]
A_23_P390148	2.87286	1.76E-04	2.1100988	0.0018770149	up	RALGPS1	Homo sapiens Ral GEF with PH domain and SH3 binding motif 1 (RALGPS1), transcript variant 1, mRNA [NM_014636]
A_21_P0014188	4.771143	2.04E-04	2.104428	0.03109262	up	LOC401317	Homo sapiens cDNA clone IMAGE:30398108. [BC087859]
A_23_P365738	2.2163196	3.45E-04	2.4580507	5.84E-04	up	ARC	Homo sapiens activity-regulated cytoskeleton-associated protein (ARC), mRNA [NM_015193]
A_23_P251075	7.625535	2.44E-04	3.648103	0.0030518444	up	MAMLD1	Homo sapiens mastermind-like domain containing 1 (MAMLD1), transcript variant 2, mRNA [NM_005491]
A_21_P0010477	4.0579357	0.0010951136	2.0789135	0.040579665	up	lnc-SYN3-1	LNCipedia lincRNA (lnc-SYN3-1), lincRNA [lnc-SYN3-1:1]
A_23_P168882	2.2588382	6.59E-04	2.2673938	8.26E-04	up	TP53INP1	Homo sapiens tumor protein p53 inducible nuclear protein 1 (TP53INP1), transcript variant 1, mRNA [NM_033285]
A_33_P3330786	2.7701626	0.016094107	2.6463683	0.033369005	up	LOC728339	PREDICTED: Homo sapiens uncharacterized LOC728339 (LOC728339), misc_RNA [XR_425830]
A_33_P3215282	9.436892	2.81E-05	2.061688	8.26E-04	up	TTBK1	Homo sapiens tau tubulin kinase 1 (TTBK1), mRNA [NM_032538]
A_33_P3293593	14.810348	9.22E-06	2.2154975	0.0011954524	up	TTC9B	Homo sapiens tetratricopeptide repeat domain 9B (TTC9B), mRNA [NM_152479]
A_33_P3221859	2.2815814	3.85E-04	2.6977224	5.83E-04	up	SHOX2	Homo sapiens short stature homeobox 2 (SHOX2), transcript variant 1, mRNA [NM_003030]
A_33_P3229171	2.7259853	0.007272733	2.7915745	0.016147928	up	FLJ44635	Homo sapiens TPT1-like protein (FLJ44635), mRNA [NM_207422]
A_23_P166929	3.68103	8.65E-04	2.0049393	0.028876524	up	SERPINI1	Homo sapiens serpin peptidase inhibitor, clade I (neuroserpin), member 1 (SERPINI1), transcript variant 1, mRNA [NM_005025]
A_23_P47728	4.8424306	2.81E-05	2.0256479	6.58E-04	up	MAP6	Homo sapiens microtubule-associated protein 6 (MAP6), transcript variant 1, mRNA [NM_033063]
A_23_P382775	3.5760055	4.73E-05	2.42425	3.57E-04	up	BBC3	Homo sapiens BCL2 binding component 3 (BBC3), transcript variant 4, mRNA [NM_014417]
A_23_P66481	2.420315	0.03732581	2.6864622	0.041435767	up	RTN4RL1	Homo sapiens reticulon 4 receptor-like 1 (RTN4RL1), mRNA [NM_178568]
A_33_P3359012	8.426767	2.81E-05	2.1204364	0.0015257756	up	DUSP8	Homo sapiens dual specificity phosphatase 8 (DUSP8), mRNA [NM_004420]
A_23_P5342	4.356923	0.0030576151	8.249947	0.0038698516	up	LRP1B	Homo sapiens low density lipoprotein receptor-related protein 1B (LRP1B), mRNA [NM_018557]
A_21_P0000471	2.7416344	0.0028867512	2.288771	0.0053224275	up	SNORD111B	Homo sapiens small nucleolar RNA, C/D box 111B (SNORD111B), small nucleolar RNA [NR_037420]
A_23_P141394	2.8732836	9.88E-05	2.3185642	3.57E-04	up	WIPI1	Homo sapiens WD repeat domain, phosphoinositide interacting 1 (WIPI1), mRNA [NM_017983]
A_24_P303524	3.2881982	3.87E-04	2.6656265	0.0019065142	up	MICALL2	Homo sapiens MICAL-like 2 (MICALL2), mRNA [NM_182924]
A_33_P3289865	2.690633	1.45E-04	2.846265	4.20E-04	up	PLCL1	Homo sapiens phospholipase C-like 1 (PLCL1), mRNA [NM_006226]
A_23_P358410	3.6714563	3.12E-04	2.8294752	0.0017107966	up	SRGAP3	Homo sapiens SLIT-ROBO Rho GTPase activating protein 3 (SRGAP3), transcript variant 1, mRNA [NM_014850]
A_23_P64785	4.950767	0.005589798	3.1177237	0.044412386	up	ZNF641	Homo sapiens zinc finger protein 641 (ZNF641), transcript variant 1, mRNA [NM_152320]
A_23_P167030	11.593486	2.58E-04	2.7310956	0.0161599	up	PTH1R	Homo sapiens parathyroid hormone 1 receptor (PTH1R), transcript variant 1, mRNA [NM_000316]
A_33_P3282390	3.5029747	8.94E-04	3.0398884	0.001343977	up	GRM4	Homo sapiens glutamate receptor, metabotropic 4 (GRM4), transcript variant 1, mRNA [NM_000841]
A_23_P359245	2.301601	0.0010938711	2.0767865	0.0027761892	up	MET	Homo sapiens MET proto-oncogene, receptor tyrosine kinase (MET), transcript variant 2, mRNA [NM_000245]
A_24_P555473	2.6368775	0.001160399	3.551906	0.005355885	up	MARCH3	Homo sapiens membrane-associated ring finger (C3HC4) 3, E3 ubiquitin protein ligase (MARCH3), mRNA [NM_178450]
A_23_P130974	6.09091	2.81E-05	2.4903197	4.27E-04	up	KIAA1683	Homo sapiens KIAA1683 (KIAA1683), transcript variant 2, mRNA [NM_025249]
A_23_P148297	4.281046	0.0058885715	2.8087895	0.041939866	up	SH3BGRL	Homo sapiens SH3 domain binding glutamate-rich protein like (SH3BGRL), mRNA [NM_003022]
A_32_P202013	2.430851	0.03959322	3.082054	9.48E-04	up	FAM196A	Homo sapiens family with sequence similarity 196, member A (FAM196A), mRNA [NM_001039762]
A_33_P3323298	2.3598409	9.06E-05	2.406259	1.83E-04	up	JUN	Homo sapiens jun proto-oncogene (JUN), mRNA [NM_002228]
A_33_P3293918	19.042671	8.13E-06	4.668224	1.15E-04	up	SH2D3C	Homo sapiens SH2 domain containing 3C (SH2D3C), transcript variant 1, mRNA [NM_170600]
A_33_P3283863	3.260648	1.84E-04	2.0664024	0.0036565284	up	TENM1	Homo sapiens teneurin transmembrane protein 1 (TENM1), transcript variant 1, mRNA [NM_001163278]
A_23_P301521	5.9798164	1.22E-04	3.9048495	0.001106154	up	KIAA1462	Homo sapiens KIAA1462 (KIAA1462), mRNA [NM_020848]
A_23_P38346	3.207148	2.46E-04	2.1894526	0.00298734	up	DHX58	Homo sapiens DEXH (Asp-Glu-X-His) box polypeptide 58 (DHX58), mRNA [NM_024119]
A_24_P273799	3.5910695	8.18E-04	2.4791858	0.0114872875	up	ZNF641	Homo sapiens zinc finger protein 641 (ZNF641), transcript variant 1, mRNA [NM_152320]
A_33_P3226775	2.825814	0.0049369787	2.3145819	0.023692247	up	MUC20	Homo sapiens mucin 20, cell surface associated (MUC20), transcript variant S, mRNA [NM_001098516]
A_33_P3387518	3.3330526	0.0036974696	3.2936265	0.015398564	up	FEZF2	Homo sapiens FEZ family zinc finger 2 (FEZF2), mRNA [NM_018008]
A_21_P0010998	3.9191034	5.52E-04	2.385387	0.008405456	up	LOC283140	
A_33_P3367984	4.1400933	7.34E-05	2.1851633	9.48E-04	up	ABCA12	Homo sapiens ATP-binding cassette, sub-family A (ABC1), member 12 (ABCA12), transcript variant 1, mRNA [NM_173076]
A_33_P3315519	2.9429574	0.013854698	3.363245	0.025902562	up	LONRF2	Homo sapiens LON peptidase N-terminal domain and ring finger 2 (LONRF2), mRNA [NM_198461]
A_23_P15174	2.053577	3.38E-04	14.144711	1.43E-05	up	MT1F	Homo sapiens metallothionein 1F (MT1F), transcript variant 1, mRNA [NM_005949]
A_23_P255672	4.846876	0.008951237	3.3923762	0.045827307	up	ABLIM2	Homo sapiens actin binding LIM protein family, member 2 (ABLIM2), transcript variant 6, mRNA [NM_032432]
A_24_P405631	3.4870365	2.13E-04	3.9587872	8.28E-05	up	FEZF2	Homo sapiens FEZ family zinc finger 2 (FEZF2), mRNA [NM_018008]
A_21_P0014217	3.3226492	2.40E-04	2.5050418	0.0019242752	up		
A_33_P3230269	2.8355527	3.77E-04	2.1583571	0.0025975339	up	GRHL1	Homo sapiens grainyhead-like 1 (Drosophila) (GRHL1), mRNA [NM_198182]
A_33_P3397150	5.172046	2.81E-05	3.2251256	1.15E-04	up	PRR36	Homo sapiens proline rich 36 (PRR36), transcript variant 1, mRNA [NM_001190467]
A_33_P3268487	2.2208502	2.97E-04	2.3244581	7.20E-04	up	ABAT	Homo sapiens 4-aminobutyrate aminotransferase (ABAT), transcript variant 2, mRNA [NM_000663]
A_33_P3231670	5.073723	3.38E-04	2.1999886	0.013580674	up	RNF208	Homo sapiens ring finger protein 208 (RNF208), mRNA [NM_031297]
A_33_P3263432	2.1653488	0.025847906	2.201201	0.00415011	up	ITGA10	Homo sapiens integrin, alpha 10 (ITGA10), transcript variant 1, mRNA [NM_003637]
A_23_P35082	2.6067839	1.52E-04	2.1426241	0.0017107966	up	SESN2	Homo sapiens sestrin 2 (SESN2), mRNA [NM_031459]
A_24_P382489	2.1231887	5.05E-04	2.0171514	5.30E-04	up	SLC27A1	solute carrier family 27 (fatty acid transporter), member 1 [Source:HGNC Symbol;Acc:HGNC:10995] [ENST00000594962]
A_23_P24457	3.3523247	2.81E-04	3.222349	0.001211439	up	LRRC4C	Homo sapiens leucine rich repeat containing 4C (LRRC4C), transcript variant 1, mRNA [NM_020929]
A_23_P356616	2.3989916	9.06E-05	2.1390688	4.17E-04	up	ABTB2	Homo sapiens ankyrin repeat and BTB (POZ) domain containing 2 (ABTB2), mRNA [NM_145804]
A_32_P183765	4.754683	2.81E-05	2.3980093	3.57E-04	up	ERBB4	Homo sapiens erb-b2 receptor tyrosine kinase 4 (ERBB4), transcript variant JM-a/CVT-1, mRNA [NM_005235]
A_33_P3245178	2.3459854	2.75E-04	2.8325744	3.57E-04	up	BEX2	Homo sapiens brain expressed X-linked 2 (BEX2), transcript variant 1, mRNA [NM_001168399]
A_24_P945283	7.762742	6.21E-05	2.0181427	0.006700424	up	DLG3	Homo sapiens discs, large homolog 3 (Drosophila) (DLG3), transcript variant 1, mRNA [NM_021120]
A_23_P152791	2.6662807	0.002533652	2.2721598	0.041939866	up	SLC16A6	Homo sapiens solute carrier family 16, member 6 (SLC16A6), transcript variant 2, mRNA [NM_004694]
A_23_P47682	3.4690661	0.0038736463	2.334831	0.031963073	up	NRIP3	Homo sapiens nuclear receptor interacting protein 3 (NRIP3), mRNA [NM_020645]
A_33_P3244274	6.0343366	2.81E-05	2.1446023	0.0017469138	up	RNF208	Homo sapiens ring finger protein 208, mRNA (cDNA clone MGC:21544 IMAGE:4151712), complete cds. [BC016958]
A_21_P0002046	2.4406724	1.30E-04	2.0813777	0.0012066868	up	SIX3-AS1	Homo sapiens SIX3 antisense RNA 1 (SIX3-AS1), transcript variant 1, long non-coding RNA [NR_103785]
A_32_P190303	2.5941918	1.34E-04	2.0799923	0.0010370406	up	LONRF2	Homo sapiens LON peptidase N-terminal domain and ring finger 2 (LONRF2), mRNA [NM_198461]
A_33_P3851174	9.988177	8.74E-05	3.2027438	0.0023496018	up	SCRT1	Homo sapiens scratch family zinc finger 1 (SCRT1), mRNA [NM_031309]
A_33_P3218960	3.7284353	1.80E-04	2.1101134	0.0030588931	up	CACNA1H	Homo sapiens calcium channel, voltage-dependent, T type, alpha 1H subunit (CACNA1H), transcript variant 1, mRNA [NM_0210
A_23_P415401	2.0489905	3.85E-04	2.5193012	6.25E-04	up	KLF9	Homo sapiens Kruppel-like factor 9 (KLF9), mRNA [NM_001206]
A_32_P119033	2.6454537	8.26E-04	2.946162	0.002020507	up	PLCXD3	Homo sapiens phosphatidylinositol-specific phospholipase C, X domain containing 3 (PLCXD3), mRNA [NM_001005473]
A_32_P10936	3.1972482	1.45E-04	4.958399	1.83E-04	up	CDH12	Homo sapiens cadherin 12, type 2 (N-cadherin 2) (CDH12), mRNA [NM_004061]
A_23_P42882	3.9236374	2.46E-04	2.261411	0.0046060323	up	CAMK2B	Homo sapiens calcium/calmodulin-dependent protein kinase II beta (CAMK2B), transcript variant 6, mRNA [NM_172082]
A_23_P325642	2.096568	0.0014273144	2.3438904	0.0032961061	up	PDIA2	Homo sapiens protein disulfide isomerase family A, member 2 (PDIA2), mRNA [NM_006849]
A_32_P75792	3.81207	1.64E-04	2.2627978	0.013630229	up	FAM132A	Homo sapiens family with sequence similarity 132, member A (FAM132A), mRNA [NM_001014980]
A_33_P3371999	2.7606356	3.87E-04	2.1416419	0.00409225	up	TPPP	Homo sapiens tubulin polymerization promoting protein (TPPP), mRNA [NM_007030]
A_33_P3235137	15.251045	1.50E-04	5.111317	0.0025798767	up	SCRT1	Homo sapiens scratch family zinc finger 1 (SCRT1), mRNA [NM_031309]
A_33_P3294608	2.7931943	1.98E-04	2.0079122	0.0016090327	up	MVP	Homo sapiens major vault protein (MVP), transcript variant 1, mRNA [NM_017458]
A_23_P31739	52.722763	8.13E-06	7.810467	1.54E-04	up	STMN4	Homo sapiens stathmin-like 4 (STMN4), transcript variant 1, mRNA [NM_030795]
A_21_P0001935	3.1481361	5.52E-04	2.097045	0.010484192	up	ERICH2	Homo sapiens glutamate-rich 2 (ERICH2), transcript variant 3, mRNA [NM_001290031]
A_21_P0002313	4.8376985	0.0042627794	3.0603776	0.0352476	up	lnc-AC007405.	LNCipedia lincRNA (lnc-AC007405.7.1-1), lincRNA [lnc-AC007405.7.1-1:1]

Table 6. BENPORATH-PRC2-TARGETS

BENPORATH_PRC2_TARGETS

NAME	PROBE	GENE SYMBOL	GENE_TITLE	RANK IN GENE LIST	RANK METRIC SCORE	RUNNING ES	CORE ENRICHMENT
row_0	JUN	null	null	10	4.7176713943481400	0.011983246	Yes
row_1	ABTB2	null	null	13	4.474986553192140	0.023788113	Yes
row_2	MNX1	null	null	15	4.404457092285160	0.0354636	Yes
row_3	MESP1	null	null	26	4.140100955963140	0.04590813	Yes
row_4	IRX4	null	null	36	3.996100425720220	0.056027543	Yes
row_5	FEZF2	null	null	37	3.9761977195739700	0.06662062	Yes
row_6	SHOX2	null	null	54	3.8168063163757300	0.07585273	Yes
row_7	CBLN1	null	null	113	3.3717026710510300	0.08144116	Yes
row_8	CHODL	null	null	164	3.1096487045288100	0.086799614	Yes
row_9	ZADH2	null	null	172	3.0674824714660600	0.09456211	Yes
row_10	SIX3	null	null	217	2.889976978302000	0.09968646	Yes
row_11	VASH1	null	null	242	2.8147616386413600	0.10578083	Yes
row_12	FAM89A	null	null	254	2.784393072128300	0.112555064	Yes
row_13	NELL1	null	null	261	2.7632782459259000	0.11956565	Yes
row_14	UCN	null	null	317	2.577712059021000	0.12321436	Yes
row_15	SLC35F3	null	null	345	2.5185000896453900	0.1283439	Yes
row_16	IGSF21	null	null	364	2.469266414642330	0.13386895	Yes
row_17	GATA6	null	null	370	2.4568982124328600	0.14012182	Yes
row_18	NKX3-2	null	null	397	2.3905282020568800	0.14496894	Yes
row_19	STMN2	null	null	440	2.3123886585235600	0.14867157	Yes
row_20	RIMKLA	null	null	450	2.299487829208370	0.15427099	Yes
row_21	HEY1	null	null	471	2.2585043907165500	0.15911752	Yes
row_22	LHX6	null	null	480	2.2457573413848900	0.16463232	Yes
row_23	SLC1A2	null	null	500	2.212364673614500	0.16941443	Yes
row_24	CTNND2	null	null	605	2.0629687309265100	0.1688243	Yes
row_25	TMEM88	null	null	612	2.054939031600950	0.17394778	Yes
row_26	BTG2	null	null	704	1.9299858808517500	0.17376412	Yes
row_27	HLX	null	null	706	1.927515983581540	0.17884074	Yes
row_28	PLXNA2	null	null	710	1.9242264032363900	0.18379155	Yes
row_29	ERBB4	null	null	785	1.8465614318847700	0.18438049	Yes
row_30	RASL10A	null	null	827	1.806360125541690	0.1867935	Yes
row_31	RYR3	null	null	832	1.8011354207992600	0.19135787	Yes
row_32	ESPN	null	null	850	1.7870632410049400	0.19512397	Yes
row_33	PIGZ	null	null	857	1.7828136682510400	0.19952248	Yes
row_34	HTR7	null	null	881	1.7622283697128300	0.20287131	Yes
row_35	KIRREL3	null	null	897	1.7539678812027000	0.20666628	Yes
row_36	KLF4	null	null	907	1.7372934818267800	0.21076795	Yes
row_37	ONECUT2	null	null	915	1.7332192659378100	0.21497582	Yes
row_38	DACH1	null	null	922	1.7275440692901600	0.21922708	Yes
row_39	VAX2	null	null	959	1.6995428800582900	0.22164813	Yes
row_40	GUCY1A3	null	null	1095	1.5885037183761600	0.21797982	Yes
row_41	HRK	null	null	1108	1.5818737745285000	0.22149187	Yes
row_42	ADAP2	null	null	1121	1.5737937688827500	0.2249824	Yes
row_43	MAPT	null	null	1139	1.557565450668340	0.22813709	Yes
row_44	KCNK12	null	null	1146	1.5470157861709600	0.23190741	Yes
row_45	CYP27B1	null	null	1193	1.5151498317718500	0.233252	Yes
row_46	ABCC8	null	null	1202	1.5081543922424300	0.23680174	Yes
row_47	ZNF503	null	null	1220	1.4888744354248000	0.23977344	Yes
row_48	NEUROD	null	null	1258	1.4616934061050400	0.24150231	Yes
row_49	TRIM67	null	null	1343	1.4058525562286400	0.24033195	Yes
row_50	GRIN3A	null	null	1506	1.3108270168304400	0.23434381	Yes

row_51	GRIA2	null	null	1518	1.3015755414962800	0.23716764	Yes
row_52	LRRTM1	null	null	1522	1.3009297847747800	0.2404579	Yes
row_53	TBX1	null	null	1553	1.2854875326156600	0.24212699	Yes
row_54	PROK2	null	null	1558	1.2811335325241100	0.245306	Yes
row_55	SIM2	null	null	1560	1.2799549102783200	0.24865744	Yes
row_56	CA10	null	null	1577	1.2742408514022800	0.25111583	Yes
row_57	DDAH1	null	null	1620	1.2546392679214500	0.25200048	Yes
row_58	ZFYVE28	null	null	1627	1.2513657808303800	0.25498316	Yes
row_59	INA	null	null	1636	1.246609091758730	0.2578361	Yes
row_60	SLCO5A1	null	null	1737	1.2058241367340100	0.2551965	Yes
row_61	KCNH1	null	null	1745	1.2031192779541000	0.25799212	Yes
row_62	FEV	null	null	1756	1.1990822553634600	0.26060143	Yes
row_63	TMEM59I	null	null	1759	1.1973625421524000	0.2636743	Yes
row_64	ATF3	null	null	1760	1.1973183155059800	0.2668641	Yes
row_65	SLITRK3	null	null	1794	1.180450201034550	0.2680778	Yes
row_66	GATA2	null	null	1861	1.1602998971939100	0.2673066	Yes
row_67	HSF4	null	null	1885	1.1490556001663200	0.26902184	Yes
row_68	PRKCE	null	null	1921	1.1352797746658300	0.26999816	Yes
row_69	NEFM	null	null	1940	1.130316972732540	0.2719561	Yes
row_70	TBX2	null	null	1972	1.1167736053466800	0.27311715	Yes
row_71	DCLK2	null	null	2031	1.0916709899902300	0.27263132	Yes
row_72	TRADD	null	null	2033	1.0912843942642200	0.27548012	Yes
row_73	LYSMD2	null	null	2048	1.0878090858459500	0.2775589	Yes
row_74	PKNOX2	null	null	2074	1.0767059326171900	0.27896434	Yes
row_75	ADRB1	null	null	2206	1.0317739248275800	0.2740469	Yes
row_76	RBP4	null	null	2253	1.0151097774505600	0.27405933	Yes
row_77	NKX6-1	null	null	2255	1.0146962404251100	0.2767041	Yes
row_78	TMEFF2	null	null	2263	1.0115315914154100	0.2789893	Yes
row_79	SLIT1	null	null	2273	1.0055423974990800	0.2811415	Yes
row_80	CACNA1I	null	null	2278	1.0021275281906100	0.2835772	Yes
row_81	SCD5	null	null	2308	0.9929313659667970	0.2845254	Yes
row_82	TP73	null	null	2351	0.9798868894577030	0.28467807	Yes
row_83	TRIM9	null	null	2359	0.976244330406189	0.28686926	Yes
row_84	GPR12	null	null	2378	0.9709592461586000	0.28840265	Yes
row_85	BHLHE22	null	null	2397	0.9632940888404850	0.2899156	Yes
row_86	RAX	null	null	2414	0.9572073817253110	0.2915294	Yes
row_87	DSCAML	null	null	2446	0.9499183893203740	0.29224595	Yes
row_88	REPS2	null	null	2500	0.9316467046737670	0.29162636	Yes
row_89	SLC32A1	null	null	2624	0.8959595561027530	0.2868153	Yes
row_90	B4GALNT	null	null	2636	0.8909521102905270	0.28854516	Yes
row_91	GATA3	null	null	2678	0.8774666786193850	0.2884835	Yes
row_92	ANKRD20	null	null	2689	0.8747882843017580	0.29022884	Yes
row_93	DGKI	null	null	2713	0.8690444231033330	0.2911981	Yes
row_94	KLHL35	null	null	2734	0.8614541888237	0.29232273	Yes
row_95	FAM19A4	null	null	2755	0.8563942313194280	0.29343385	Yes
row_96	POLE	null	null	2793	0.8464403748512270	0.2935236	Yes
row_97	CDK5R2	null	null	2855	0.830448567867279	0.29216626	Yes
row_98	CLCN5	null	null	2903	0.817176342010498	0.29159284	Yes
row_99	ZFHX3	null	null	2924	0.8096243143081670	0.29257938	Yes
row_100	ANKRD27	null	null	2938	0.8070215582847600	0.29396862	Yes
row_101	TLX1	null	null	2947	0.8059882521629330	0.29564768	Yes
row_102	MT1M	null	null	2956	0.8032759428024290	0.29731956	Yes
row_103	KCNAB1	null	null	2960	0.8021692037582400	0.29928106	Yes
row_104	FAM84A	null	null	3004	0.7893899083137510	0.2988677	No
row_105	PAX2	null	null	3107	0.7637913227081300	0.29493344	No

row_106	CDKN2C	null	null	3130	0.7583194971084600	0.29566625	No
row_107	TBX5	null	null	3228	0.7355260848999020	0.29194927	No
row_108	SPOCK3	null	null	3242	0.732003927230835	0.29313865	No
row_109	KCNMA1	null	null	3280	0.7224599719047550	0.29289812	No
row_110	ECEL1	null	null	3297	0.7182459235191350	0.29387528	No
row_111	HS3ST3B	null	null	3354	0.7051848769187930	0.29247683	No
row_112	EGR4	null	null	3407	0.6937851309776310	0.2912821	No
row_113	POU4F2	null	null	3441	0.6862058639526370	0.29117903	No
row_114	CDH23	null	null	3461	0.6813123226165770	0.29188225	No
row_115	NRG2	null	null	3464	0.6808829307556150	0.29357916	No
row_116	NPTX1	null	null	3497	0.6734927296638490	0.29350078	No
row_117	ANKRD18	null	null	3536	0.6637670397758480	0.29304534	No
row_118	F2R	null	null	3543	0.661768913269043	0.29445726	No
row_119	SEMA6D	null	null	3570	0.6543847918510440	0.29467908	No
row_120	NCAM1	null	null	3587	0.6512258052825930	0.2954777	No
row_121	DUSP4	null	null	3607	0.6470268368721010	0.29608956	No
row_122	GRIK3	null	null	3685	0.6299059987068180	0.29326162	No
row_123	NRG1	null	null	3694	0.6273961067199710	0.29446492	No
row_124	PRDM12	null	null	3712	0.6240469217300420	0.2951326	No
row_125	METRNL	null	null	3760	0.6124871373176580	0.2940139	No
row_126	SSTR2	null	null	3807	0.6040796637535100	0.29293126	No
row_127	RAB6C	null	null	3823	0.602057158946991	0.29365742	No
row_128	PPM1E	null	null	3825	0.6011461019515990	0.2952004	No
row_129	PTGFR	null	null	3841	0.5971816778182980	0.29591358	No
row_130	ANKRD19	null	null	3864	0.5923301577568050	0.29620415	No
row_131	FGF20	null	null	3931	0.578618049621582	0.29388332	No
row_132	HHIP	null	null	3941	0.5762614607810970	0.29489186	No
row_133	PRKG1	null	null	3985	0.5664952993392940	0.2938847	No
row_134	ZEB2	null	null	4004	0.5633693933486940	0.2943322	No
row_135	POU3F4	null	null	4043	0.5550557971000670	0.29358715	No
row_136	MT1A	null	null	4074	0.5495781302452090	0.29329568	No
row_137	HBA2	null	null	4114	0.5426086187362670	0.29245895	No
row_138	PDE4DIP	null	null	4146	0.5349529385566710	0.29207	No
row_139	HOXD1	null	null	4174	0.5293973684310910	0.2919003	No
row_140	SHC4	null	null	4208	0.5235325694084170	0.2913639	No
row_141	ANKRD18	null	null	4217	0.5217394232749940	0.2922857	No
row_142	HS6ST3	null	null	4230	0.5202102065086370	0.29296935	No
row_143	TMEM132	null	null	4256	0.5138837695121770	0.29287538	No
row_144	FGF9	null	null	4268	0.5117321014404300	0.293595	No
row_145	PDGFRA	null	null	4301	0.5054278373718260	0.29306883	No
row_146	MAPK4	null	null	4361	0.4947597086429600	0.29093423	No
row_147	CHST8	null	null	4415	0.4848496615886690	0.28912434	No
row_148	SLC30A4	null	null	4502	0.4685196876525880	0.28533974	No
row_149	NAV2	null	null	4608	0.4480965733528140	0.28038886	No
row_150	SGPP2	null	null	4614	0.44663506746292100	0.28128615	No
row_151	RTN4RL2	null	null	4616	0.4463236629962920	0.2824167	No
row_152	LTK	null	null	4631	0.4433150589466100	0.28277847	No
row_153	DLX4	null	null	4645	0.4404872953891750	0.2831912	No
row_154	NEUROD2	null	null	4647	0.43964603543281600	0.28430396	No
row_155	NOL4	null	null	4662	0.436381071805954	0.28464723	No
row_156	ST8SIA2	null	null	4675	0.43322259187698400	0.28509915	No
row_157	OCA2	null	null	4716	0.42443814873695400	0.28388909	No
row_158	NBPF11	null	null	4756	0.4197424650192260	0.282725	No
row_159	ADRB3	null	null	4764	0.41683229804039	0.28342587	No
row_160	GBX2	null	null	4802	0.4085933268070220	0.28234914	No

row_161	GATA4	null	null	4805	0.4083620607852940	0.28332004	No
row_162	MT1B	null	null	4806	0.408314049243927	0.28440782	No
row_163	RGS20	null	null	4824	0.404005229473114	0.2844893	No
row_164	PLEC	null	null	4825	0.4039986729621890	0.2855656	No
row_165	TMEM27	null	null	4898	0.3914619982242580	0.28239504	No
row_166	ANKRD2(	null	null	4902	0.3905641436576840	0.28325996	No
row_167	WNT10B	null	null	4937	0.38568615913391100	0.2822978	No
row_168	POU4F1	null	null	4950	0.3819430470466610	0.28261307	No
row_169	EFNA1	null	null	4957	0.3799576163291930	0.2832742	No
row_170	WT1	null	null	5172	0.345045804977417	0.27167004	No
row_171	TTYH1	null	null	5179	0.34391501545906100	0.27223516	No
row_172	C2CD4A	null	null	5266	0.32888343930244400	0.26807857	No
row_173	NTNG2	null	null	5321	0.31991007924079900	0.26577073	No
row_174	CSMD1	null	null	5329	0.3192513883113860	0.26621163	No
row_175	PITX2	null	null	5331	0.3191165626049040	0.26700327	No
row_176	EPHB3	null	null	5367	0.31246471405029300	0.26578748	No
row_177	WNT6	null	null	5380	0.3102514147758480	0.2659118	No
row_178	LPHN3	null	null	5412	0.30547624826431300	0.26491147	No
row_179	ANKRD2(	null	null	5438	0.3012167811393740	0.26425093	No
row_180	AQP5	null	null	5480	0.2932738661766050	0.2626329	No
row_181	FBXL8	null	null	5534	0.28291115164756800	0.26028502	No
row_182	SHOX	null	null	5546	0.2816697955131530	0.2603917	No
row_183	CRYBA2	null	null	5606	0.27334511280059800	0.2576672	No
row_184	KIAA1324	null	null	5750	0.25024574995040900	0.24996544	No
row_185	BARX1	null	null	5752	0.2501353621482850	0.2505733	No
row_186	BATF3	null	null	5822	0.23848669230938000	0.24717076	No
row_187	RGS10	null	null	5873	0.23135343194007900	0.24486108	No
row_188	CBR3	null	null	5944	0.22107696533203100	0.24135362	No
row_189	WNT10A	null	null	6010	0.2116645872592930	0.23811367	No
row_190	SLC1A4	null	null	6160	0.1900928020477300	0.22990054	No
row_191	IL7	null	null	6364	0.16164366900920900	0.21845149	No
row_192	DPF3	null	null	6401	0.1585427075624470	0.21676713	No
row_193	SLC27A2	null	null	6429	0.15571816265583000	0.21560192	No
row_194	SYT12	null	null	6483	0.14734891057014500	0.21289289	No
row_195	FOXD2	null	null	6510	0.14218378067016600	0.21175015	No
row_196	ISL2	null	null	6586	0.13135044276714300	0.20771104	No
row_197	RIMBP3	null	null	6639	0.12325886636972400	0.20499633	No
row_198	CASZ1	null	null	6673	0.11762523651123000	0.20337853	No
row_199	CACNA1(	null	null	6693	0.11481720954179800	0.20257252	No
row_200	MAFB	null	null	6723	0.11088596284389500	0.20117085	No
row_201	NTRK1	null	null	6776	0.10274213552475000	0.19840148	No
row_202	OTOP2	null	null	6790	0.10036521404981600	0.1979081	No
row_203	ITPKA	null	null	6795	0.09991662949323650	0.19794022	No
row_204	COMP	null	null	6812	0.09760671108961110	0.19726391	No
row_205	SLIT2	null	null	6887	0.08799200505018230	0.19316782	No
row_206	DLX2	null	null	6982	0.07438812404870990	0.18786506	No
row_207	CNNM1	null	null	7113	0.05481636896729470	0.18040341	No
row_208	ZIC4	null	null	7164	0.047735512256622300	0.17760456	No
row_209	DOK6	null	null	7172	0.04634098708629610	0.17731838	No
row_210	LRP2	null	null	7235	0.03623053431510930	0.17378663	No
row_211	PHOX2A	null	null	7333	0.022943036630749700	0.16817124	No
row_212	HOXC8	null	null	7360	0.019389791414141700	0.16670136	No
row_213	DNAJC22	null	null	7423	0.011756550520658500	0.16310441	No
row_214	LMX1B	null	null	7435	0.009803281165659430	0.1624868	No
row_215	CDH7	null	null	7440	0.009300339967012410	0.16227749	No

row_216	ANKRD2(	null	null	7483	0.0020042373798787600	0.15982497	No
row_217	HOXC4	null	null	7539	-0.007023638114333150	0.15662505	No
row_218	ATOH8	null	null	7597	-0.017166974022984500	0.15333511	No
row_219	RPS6KA6	null	null	7617	-0.020296838134527200	0.15227729	No
row_220	GDNF	null	null	7650	-0.026431387290358500	0.15047505	No
row_221	NEFL	null	null	7660	-0.02775612287223340	0.15002231	No
row_222	DPY19L2	null	null	7682	-0.030051739886403100	0.14887343	No
row_223	LGALS3	null	null	7691	-0.03167131543159490	0.14848965	No
row_224	IRX5	null	null	7701	-0.03332742676138880	0.14805175	No
row_225	HOXC6	null	null	7722	-0.03673442453145980	0.1469792	No
row_226	MYO5B	null	null	7731	-0.037701647728681600	0.14661148	No
row_227	ALX4	null	null	7792	-0.04765557125210760	0.1432272	No
row_228	WRAP73	null	null	7797	-0.04817042499780660	0.14312145	No
row_229	GSC	null	null	7947	-0.06884488463401790	0.13458529	No
row_230	PTGER3	null	null	7951	-0.06937148422002790	0.13459454	No
row_231	NKX2-3	null	null	8026	-0.08157864958047870	0.13048136	No
row_232	TCEA3	null	null	8152	-0.09946943819522860	0.12343128	No
row_233	OLFML2E	null	null	8181	-0.10417528450489000	0.122070245	No
row_234	CITED1	null	null	8247	-0.11388690024614300	0.11856981	No
row_235	PITX1	null	null	8288	-0.11808807402849200	0.11654359	No
row_236	ZNF436	null	null	8332	-0.12244807928800600	0.11435342	No
row_237	STXBP6	null	null	8459	-0.14101016521453900	0.10735549	No
row_238	UNC5C	null	null	8480	-0.14380362629890400	0.10656819	No
row_239	ANKRD2(	null	null	8691	-0.17348173260688800	0.09474104	No
row_240	EPB41L4A	null	null	8696	-0.17420408129692100	0.09497106	No
row_241	INSM2	null	null	8709	-0.17589068412780800	0.09473741	No
row_242	HAND2	null	null	8810	-0.1893617808818820	0.08938983	No
row_243	EPHB1	null	null	8948	-0.20619811117649100	0.081921846	No
row_244	STK32B	null	null	8980	-0.21137607097625700	0.08067084	No
row_245	ICAM5	null	null	9030	-0.21920040249824500	0.078387305	No
row_246	HOXD9	null	null	9164	-0.23943954706192000	0.07124196	No
row_247	CD8A	null	null	9172	-0.24110464751720400	0.07147465	No
row_248	PAX6	null	null	9192	-0.24453367292881000	0.071014225	No
row_249	HPSE2	null	null	9193	-0.24462302029132800	0.07166593	No
row_250	HOXD3	null	null	9272	-0.2536433935165410	0.06777706	No
row_251	FOXD3	null	null	9353	-0.2655566930770870	0.06380289	No
row_252	NAGS	null	null	9430	-0.27481868863105800	0.060087472	No
row_253	HOXC5	null	null	9558	-0.2922047972679140	0.053433824	No
row_254	OPRD1	null	null	9592	-0.2973104417324070	0.052294716	No
row_255	PITX3	null	null	9669	-0.3074905276298520	0.048666343	No
row_256	PAPPA	null	null	9721	-0.313394695520401	0.046516716	No
row_257	SUSD4	null	null	9762	-0.318206250667572	0.04502363	No
row_258	CORO6	null	null	9796	-0.32252082228660600	0.043951686	No
row_259	MCOLN3	null	null	9878	-0.3326384425163270	0.040097706	No
row_260	GDF6	null	null	9923	-0.3411020338535310	0.038431536	No
row_261	NPNT	null	null	9938	-0.3432674705982210	0.038526755	No
row_262	NEUROG1	null	null	9945	-0.34443017840385400	0.039093237	No
row_263	CXCL14	null	null	10044	-0.35771435499191300	0.034311213	No
row_264	FAM163A	null	null	10049	-0.35868749022483800	0.035032716	No
row_265	PTPRU	null	null	10050	-0.35905081033706700	0.035989273	No
row_266	ARL 9.00	null	null	10097	-0.36467212438583400	0.034268856	No
row_267	CRTAC1	null	null	10105	-0.36531883478164700	0.034832466	No
row_268	NEUROG	null	null	10133	-0.36955055594444300	0.034236938	No
row_269	SOX7	null	null	10203	-0.3788856565952300	0.031208413	No
row_270	FGF5	null	null	10210	-0.3794800341129300	0.03186827	No

row_271	FZD2	null	null	10359	-0.4003535509109500	0.02427381	No
row_272	MAB21L1	null	null	10375	-0.4037121832370760	0.024471542	No
row_273	KCND3	null	null	10469	-0.420799195766449	0.020150186	No
row_274	DRD5	null	null	10497	-0.4251957833766940	0.019702902	No
row_275	SIX2	null	null	10572	-0.43587517738342300	0.016533604	No
row_276	CHRDL2	null	null	10609	-0.440570205450058	0.015600595	No
row_277	LGR5	null	null	10715	-0.453240305185318	0.010663419	No
row_278	PCDH8	null	null	10736	-0.45618781447410600	0.010708347	No
row_279	NEUROG2	null	null	10802	-0.463241308927536	0.008138639	No
row_280	NR4A3	null	null	10923	-0.48237067461013800	0.0024012611	No
row_281	HSPA6	null	null	10948	-0.48614636063575700	0.00229192	No
row_282	LBX1	null	null	11016	-0.4986574947834020	-3.004761E-04	No
row_283	ADRA1A	null	null	11108	-0.5117506384849550	-0.0042624846	No
row_284	KCNH3	null	null	11217	-0.5259479880332950	-0.00918152	No
row_285	FLRT2	null	null	11624	-0.5901845097541810	-0.03136856	No
row_286	BHLHE23	null	null	11659	-0.5945379734039310	-0.03177434	No
row_287	COL27A1	null	null	11674	-0.5978865027427670	-0.031000786	No
row_288	ZIC1	null	null	11716	-0.6041648983955380	-0.031790562	No
row_289	ZBTB16	null	null	11836	-0.6209893226623540	-0.03710012	No
row_290	VSX1	null	null	11840	-0.6214129328727720	-0.035620164	No
row_291	TRIM36	null	null	11992	-0.6427526473999020	-0.0427444	No
row_292	KCNQ3	null	null	11998	-0.6439811587333680	-0.04132136	No
row_293	SLC30A3	null	null	12107	-0.6588231325149540	-0.0458864	No
row_294	HOXD13	null	null	12131	-0.6626905202865600	-0.045466885	No
row_295	CBX8	null	null	12132	-0.6627928614616390	-0.043701123	No
row_296	COL9A2	null	null	12300	-0.6893271803855900	-0.051637612	No
row_297	ISL1	null	null	12305	-0.6896635293960570	-0.050034348	No
row_298	ESX1	null	null	12327	-0.6925128698349000	-0.04941834	No
row_299	HHEX	null	null	12438	-0.7105174660682680	-0.053962704	No
row_300	DLX1	null	null	12465	-0.7140259146690370	-0.053581987	No
row_301	SIX1	null	null	12472	-0.7150512933731080	-0.052028127	No
row_302	LPPR1	null	null	12526	-0.7240081429481510	-0.053200874	No
row_303	CYP26C1	null	null	12547	-0.7278770804405210	-0.05243213	No
row_304	HHAT	null	null	12575	-0.7330502271652220	-0.05205925	No
row_305	PXMP2	null	null	12612	-0.7374110221862790	-0.052201442	No
row_306	GPR88	null	null	12613	-0.7375397682189940	-0.050236546	No
row_307	HOXB13	null	null	12700	-0.7507213950157170	-0.053269304	No
row_308	OTP	null	null	12837	-0.774875283241272	-0.05916374	No
row_309	LAYN	null	null	12870	-0.7830294966697690	-0.058950316	No
row_310	CMTM2	null	null	12901	-0.7874810695648190	-0.058607988	No
row_311	KAZALD1	null	null	12941	-0.7964979410171510	-0.058768325	No
row_312	NKX3-1	null	null	13012	-0.8068563938140870	-0.060715202	No
row_313	MSC	null	null	13041	-0.8121364712715150	-0.06019015	No
row_314	SLC6A3	null	null	13065	-0.8175769448280330	-0.059358	No
row_315	OTX1	null	null	13218	-0.8460106253623960	-0.065999255	No
row_316	DIO3	null	null	13253	-0.8533698320388790	-0.06571548	No
row_317	NR2F2	null	null	13283	-0.8588008284568790	-0.06512462	No
row_318	SLITRK1	null	null	13432	-0.8904091119766240	-0.07141351	No
row_319	CALCA	null	null	13449	-0.8942917585372930	-0.06996734	No
row_320	PCDH17	null	null	13598	-0.9209555983543400	-0.07617485	No
row_321	CNTFR	null	null	13705	-0.9424275755882260	-0.07986729	No
row_322	ADRA2A	null	null	13761	-0.9532469511032100	-0.08054636	No
row_323	IGF2-AS	null	null	13893	-0.9793804883956910	-0.08560337	No
row_324	ITGA4	null	null	13925	-0.9850107431411740	-0.08479332	No
row_325	FOXB1	null	null	13927	-0.9851928949356080	-0.08222716	No

row_326	LHX2	null	null	13985	-0.9991588592529300	-0.082900956	No
row_327	CLSTN2	null	null	14150	-1.033486008644100	-0.08974501	No
row_328	FBXO3	null	null	14214	-1.0457946062088000	-0.09064568	No
row_329	KCNK2	null	null	14218	-1.0474827289581300	-0.08803062	No
row_330	HES2	null	null	14229	-1.0492902994155900	-0.085820384	No
row_331	OTOP1	null	null	14241	-1.0520228147506700	-0.0836614	No
row_332	TMOD2	null	null	14456	-1.0982491970062300	-0.09325894	No
row_333	SSTR1	null	null	14515	-1.114929437637330	-0.093682826	No
row_334	PMP22	null	null	14532	-1.1180028915405300	-0.09164066	No
row_335	PHOX2B	null	null	14544	-1.1215417385101300	-0.08929646	No
row_336	GRID1	null	null	14551	-1.1226778030395500	-0.08665663	No
row_337	TBX3	null	null	14765	-1.176844596862790	-0.09598626	No
row_338	NTRK2	null	null	15052	-1.2499526739120500	-0.10939313	No
row_339	OAF	null	null	15221	-1.3000398874282800	-0.11576112	No
row_340	TLX2	null	null	15262	-1.3140119314193700	-0.11460126	No
row_341	PIR	null	null	15292	-1.3270593881607100	-0.11276291	No
row_342	CHRD	null	null	15295	-1.3286789655685400	-0.10934019	No
row_343	KCNK13	null	null	15317	-1.336939811706540	-0.107007354	No
row_344	BCL2	null	null	15329	-1.3400660753250100	-0.10408098	No
row_345	ADARB2	null	null	15337	-1.3430945873260500	-0.10091246	No
row_346	COL25A1	null	null	15363	-1.3519774675369300	-0.098773636	No
row_347	EN2	null	null	15417	-1.3700107336044300	-0.098225355	No
row_348	ONECUT1	null	null	15472	-1.390567421913150	-0.09768082	No
row_349	MLLT3	null	null	15514	-1.402066707611080	-0.096344896	No
row_350	FRMD3	null	null	15547	-1.4120763540267900	-0.09445561	No
row_351	FLI1	null	null	15600	-1.4286251068115200	-0.09369265	No
row_352	ROBO3	null	null	15602	-1.429115891456600	-0.08994383	No
row_353	SORCS1	null	null	15774	-1.4927904605865500	-0.09597388	No
row_354	PDZD2	null	null	15801	-1.5020315647125200	-0.09349382	No
row_355	CNRIP1	null	null	15844	-1.521783471107480	-0.091897465	No
row_356	EPAS1	null	null	15879	-1.5381804704666100	-0.08978927	No
row_357	ADCY4	null	null	15930	-1.5587390661239600	-0.08856263	No
row_358	LRCH2	null	null	15931	-1.558939814567570	-0.08440942	No
row_359	PRLHR	null	null	15946	-1.5679891109466600	-0.081051394	No
row_360	SLC10A4	null	null	15975	-1.5806587934494000	-0.0784789	No
row_361	RSPO2	null	null	16011	-1.5945603847503700	-0.07627902	No
row_362	CRLF1	null	null	16172	-1.6656551361084000	-0.08120481	No
row_363	WNT11	null	null	16234	-1.6964107751846300	-0.08025512	No
row_364	POU3F1	null	null	16349	-1.760562539100650	-0.08223612	No
row_365	FOXF1	null	null	16361	-1.7736154794693000	-0.07815472	No
row_366	LHX8	null	null	16388	-1.787920355796810	-0.07491302	No
row_367	PTGER2	null	null	16427	-1.810186505317690	-0.07231424	No
row_368	MYOD1	null	null	16433	-1.8129960298538200	-0.0677768	No
row_369	DKK 1.00	null	null	16481	-1.8488175868988000	-0.065601796	No
row_370	GPM6B	null	null	16574	-1.919360876083370	-0.06587228	No
row_371	MSX1	null	null	16766	-2.109907865524290	-0.071428664	No
row_372	MAB21L2	null	null	16812	-2.160632610321050	-0.0683059	No
row_373	SFRP1	null	null	16870	-2.2556371688842800	-0.06563228	No
row_374	FBP1	null	null	16920	-2.321707010269170	-0.06231448	No
row_375	TET2	null	null	16923	-2.324014902114870	-0.056240063	No
row_376	RPRML	null	null	17074	-2.582913637161260	-0.05813696	No
row_377	FGF3	null	null	17269	-3.159773349761960	-0.061071932	No
row_378	SORCS3	null	null	17321	-3.343334674835210	-0.055149432	No
row_379	AGPAT9	null	null	17355	-3.5131075382232700	-0.047721267	No
row_380	ASTN2	null	null	17369	-3.5889716148376500	-0.038920578	No

row_381	PAX7	null	null	17388	-3.6979968547821000	-0.030122032	No
row_382	FOXL1	null	null	17420	-4.0655107498168900	-0.021105155	No
row_383	HOXD8	null	null	17421	-4.074563980102540	-0.010250021	No
row_384	ASCL1	null	null	17464	-4.94577693939209	4.6826628E-04	No

Table 7. sh205_206_UP_gsea_report, sh205_206_DOWN_gsea_report

sh205_206_UP_gsea_report

NAME	GS follow link to MSigDB	SIZE	ES	NES	NOM p-val	FDR q-val	FWER p-val	RANK AT MA	LEADING EDGE
GO_PANCREAS_DEVELOPMENT	GO_PANCREAS_DEVELOPMENT	48	0.585226	2.2460072	0	0.013076901	0.013	1603	tags=29%, list=9%, signal=32%
ODONNELL_TARGETS_OF_MYC_AND_TFRC_UP	ODONNELL_TARGETS_OF_MYC_AND_TFRC_UP	50	0.5758761	2.1654475	0	0.012520148	0.026	838	tags=24%, list=5%, signal=25%
GO_ENDOCRINE_PANCREAS_DEVELOPMENT	GO_ENDOCRINE_PANCREAS_DEVELOPMENT	29	0.66614217	2.1405768	0	0.011189548	0.026	1603	tags=38%, list=9%, signal=42%
GO_ENTEROENDOCRINE_CELL_DIFFERENTIATION	GO_ENTEROENDOCRINE_CELL_DIFFERENTIATION	15	0.82600415	2.0107949	0	0.03279096	0.103	1603	tags=47%, list=9%, signal=51%
MCMURRAY_TP53_HRAS_COOPERATION_RESPONSE_D	MCMURRAY_TP53_HRAS_COOPERATION_RESPONSE_D	51	0.49564606	1.9813601	0	0.037010826	0.133	1762	tags=31%, list=10%, signal=35%
HAN_JNK_SINGALING_UP	HAN_JNK_SINGALING_UP	28	0.6836551	1.9760466	0	0.03408512	0.143	1494	tags=43%, list=9%, signal=47%
WARTERS_IR_RESPONSE_5GY	WARTERS_IR_RESPONSE_5GY	35	0.5264556	1.957826	0	0.04143685	0.206	2498	tags=34%, list=14%, signal=40%

sh205_206_DOWN_gsea_report

NAME	GS follow link to MSigDB	SIZE	ES	NES	NOM p-val	FDR q-val	FWER p-val	RANK AT MA	LEADING EDGE
GO_NEURAL_NUCLEUS_DEVELOPMENT	GO_NEURAL_NUCLEUS_DEVELOPMENT	50	-0.5295738	-2.1361518	0	0.024129285	0.023	2571	tags=38%, list=15%, signal=44%
PLASARI_TGFB1_SIGNALING_VIA_NFIC_1HR_UP	PLASARI_TGFB1_SIGNALING_VIA_NFIC_1HR_UP	22	-0.5612298	-2.1281955	0	0.016787153	0.033	1242	tags=27%, list=7%, signal=29%
PID_HNF3B_PATHWAY	PID_HNF3B_PATHWAY	24	-0.5857364	-2.0925105	0	0.02315506	0.069	1237	tags=38%, list=7%, signal=40%
GO_NUCLEAR_MATRIX	GO_NUCLEAR_MATRIX	90	-0.49923426	-2.0839562	0	0.01953863	0.075	2560	tags=32%, list=15%, signal=38%
GO_SYNAPTONEMAL_COMPLEX	GO_SYNAPTONEMAL_COMPLEX	19	-0.59429806	-2.0259712	0	0.038642544	0.136	1301	tags=32%, list=7%, signal=34%
GNF2_TDG	GNF2_TDG	35	-0.7679353	-2.0198371	0	0.0348444	0.146	1852	tags=54%, list=11%, signal=61%
GO_NUCLEAR_PERIPHERY	GO_NUCLEAR_PERIPHERY	113	-0.51486015	-2.014161	0	0.032865737	0.146	3891	tags=43%, list=22%, signal=55%
GO_NEGATIVE_REGULATION_OF_MYELOID_CELL_DIFI	GO_NEGATIVE_REGULATION_OF_MYELOID_CELL_D	66	-0.49630025	-2.01042	0	0.030428827	0.148	2749	tags=35%, list=16%, signal=41%
BILANGES_SERUM_SENSITIVE_VIA_TSC1	BILANGES_SERUM_SENSITIVE_VIA_TSC1	17	-0.540373	-1.9956753	0	0.034203503	0.188	653	tags=29%, list=4%, signal=31%
ACEVEDO_LIVER_CANCER_WITH_H3K27ME3_DN	ACEVEDO_LIVER_CANCER_WITH_H3K27ME3_DN	143	-0.44622687	-1.9928726	0	0.032368366	0.191	2516	tags=29%, list=14%, signal=34%
GCTNWTTGK_UNKNOWN	GCTNWTTGK_UNKNOWN	97	-0.468068	-1.9924444	0	0.029995777	0.195	1713	tags=23%, list=10%, signal=25%
REACTOME_GLUTATHIONE_CONJUGATION	REACTOME_GLUTATHIONE_CONJUGATION	16	-0.58705133	-1.9900713	0	0.02815606	0.195	2054	tags=44%, list=12%, signal=50%
E2F4DP1_01	E2F4DP1_01	216	-0.5340137	-1.9828213	0	0.027342435	0.197	3162	tags=42%, list=18%, signal=51%

Table 8. IC50 results of valproic acid (VPA), EED226, and Suberanilohydroxamic acid (SAHA) in NGP and IMR32 cells

Drug	NGP	IMR32
Valproic acid (IC50)	7.98 mM	1.55 mM
EED226 (IC50)	2.64 μM	2.05 μM
Suberanilohydroxamic acid (IC50)	1.52 μM	0.59 μM